https://doi.org/10.5194/egusphere-2026-3607
Preprint. Discussion started: 30 June 2026


# Biogeochemistry of methane in Arctic waters: A multiyear synthesis (2014-2022) from the North Atlantic-Arctic sector and Barents Sea

Muhammed Fatih Sert[1*], Knut Ola Dølven[1], Stefan Bünz[1], Helge Niemann[2,3], Giuliana Panieri[1,4], Henry Patton[1], Andreia Plaza-Faverola[1], Tine L. Rasmussen[1], Marie Stetzler[1], Monica Winsborrow[1] and Bénédicte Ferré[1]

[1]Department of Geosciences, UiT-The Arctic University of Norway, Tromsø, Norway
[2]NIOZ Royal Institute for Sea Research, Department of Marine Microbiology and Biogeochemistry, and Utrecht University, Texel, the Netherlands
[3]Department of Earth Sciences, Faculty of Geosciences, Utrecht University, Utrecht, the Netherlands
[4]CNR-ISP Consiglio Nazionale delle Ricerche, Istituto di Scienze Polari, Venice, Italy

*Correspondence to*: Muhammed Fatih Sert (muhammed.f.sert@uit.no)

**Abstract.** Methane seeping from numerous point sources at the seabed represents a biogeochemically constrained carbon source in the water column of the Arctic Ocean. Here, we compile and synthesise water-column data from 28 research cruises conducted between 2014 and 2022 to evaluate the spatial distribution and variability of methane across Arctic seep systems and to assess whether methane enrichment produces detectable changes in water-column biogeochemistry. Our synthesis shows that methane concentrations span five orders of magnitude, ranging from non-detectable levels (<0.52 nM) to $10^5$ nM. Despite this distinct variability, continuous seeping of methane does not measurably alter bulk nutrient regimes, but it influences organic matter cycling through microbial methane oxidation (MOx). In contrast, nutrient and carbon biogeochemistry appear closely associated with seasonal patterns in primary production, showing typical vertical profiles, even in regions of maximum methane flux. This reflects the relatively low abundance of methane compared to other substrates, as nutrients and dissolved organic carbon concentrations remain one to two orders of magnitude higher even at peak methane levels. Consequently, methane-derived carbon constitutes only a minor fraction of total biogeochemical pools, constraining its effect on nutrient dynamics. However, methane exerts a cumulative influence by altering microbial processes and carbon transformation pathways, even in the absence of detectable changes in bulk nutrient concentrations.

https://doi.org/10.5194/egusphere-2026-3607
Preprint. Discussion started: 30 June 2026


## 1 Introduction

The Arctic continental margin stores vast amounts of methane in gas hydrate deposits (Mienert et al., 2022), submerged permafrost, and deep geological reservoirs, representing an important and dynamic component of the global carbon cycle (Andreassen et al., 2017; Egger et al., 2018; Portnov et al., 2013, 2014, 2016; Serov et al., 2015, 2024; Smith et al., 2014; Westbrook et al., 2009). Under changing environmental conditions, such as ocean temperature and postglacial seabed response, methane is released from these deposits (El bani Altuna, 2021; Serov et al., 2024), forming seeps and fostering the development of dynamic, methane-driven ecosystems within the overlying water column (Åström et al., 2016; Boetius and Wenzhöfer, 2013; Melaniuk et al., 2022; Sen et al., 2018). Arctic cold seeps are controlled by sediment instabilities, thawing of subsea permafrost, glacial retreat (Portnov et al., 2016), fracturing, changing tectonic stress (Cooke et al., 2023), and variations in the boundary conditions of the Gas Hydrate Stability Zone (GHSZ) (Ferré et al., 2020c; Rasmussen et al., 2024; Rasmussen and Nielsen, 2024; Sahling et al., 2014). These are mainly governed by temperature and pressure, which makes Arctic cold seeps sensitive to climate change-driven bottom-water warming, sea level change, tidal pressure variability (Sultan et al., 2020), isostatic rebound (Wallmann et al., 2018), and seasonal changes in bottom water temperature and seepage patterns (Berndt et al., 2014; Ferré et al., 2020c; James et al., 2016; Shakhova et al., 2010; Westbrook et al., 2009).

Despite the growing recognition of methane from biogenic (Egger et al., 2018) and abiotic sources (e.g., Böttner et al., 2025; Johnson et al., 2015), our understanding of methane seepage dynamics and the fate of methane in the water column remains limited. Most existing studies are centred on individual seep systems and rely on spatially constrained observations. However, seeping methane is subject to rapid dilution, complex transport pathways, and both geologic and hydrographic controls (Ferré et al., 2020c), which create highly heterogeneous distribution patterns that challenge the representativeness of seep-centred measurements. As such, extrapolations based on limited spatial coverage may lead to biased estimates of methane turnover and fate in Arctic marine systems (Dølven et al., 2022; Thornton et al., 2016).

One of the critical processes governing the fate of methane in the water column is microbial oxidation of methane (MOx) (Hanson and Hanson, 1996; Reeburgh, 2007). Depending on the environmental conditions, MOx can act as an efficient biological filter limiting methane transfer to the atmosphere. Notably, atmospheric methane measurements above some Arctic seep regions show no significant enhancement (Myhre et al., 2016) in areas with undersaturated surface water, indicating efficient methane removal within the water column (Silyakova et al., 2020). High atmospheric emissions from other areas of the Arctic, such as the East Siberian Arctic Shelves, are well documented, yet quantitative estimates diverge widely due to sparse sampling and high field heterogeneity (Berchet et al., 2016; Shakhova et al., 2010, 2014; Thornton et al., 2016). Major challenges remain in modelling methane-oxidising bacterial (MOB) communities and their efficacy, which is not fully understood and depends on a wide range of environmental factors (Crespo-Medina et al., 2014; de Groot et al., 2024; Reeburgh, 2007). Additionally, methane concentrations are low compared to those of other micronutrients and rapidly dilute away from the source. Water-column hydrography therefore, plays a fundamental role in regulating methane availability and, in turn, MOB activity and persistence (Steinle et al., 2015) . In regions where water-column hydrography is highly dynamic or unstable, methane rapidly dilutes, and MOB species may not take

https://doi.org/10.5194/egusphere-2026-3607
Preprint. Discussion started: 30 June 2026


up methane, resulting in lower MOx. Conversely, in areas with relatively stable hydrography, MOB can enhance methane oxidation and effectively compete with other microbial species (Gründger et al., 2021; Sert et al., 2020; Steinle et al., 2015). For these reasons, the fate of dissolved methane in the water column remains largely unresolved.

Beyond its role as a greenhouse gas in submarine gas hydrates (Nisbet, 2022), methane exerts a broader influence on marine biogeochemistry by entering microbial and benthic food webs (e.g., Åström et al., 2018, 2020). Methane-derived carbon is assimilated into microbial biomass or oxidised to carbon dioxide, thereby linking methane cycling to both organic and inorganic carbon pools (Hanson and Hanson, 1996). In most marine environments, the methane-driven inorganic carbon flux is considered negligible relative to fluxes associated with organic matter remineralisation. Nevertheless, even modest, localised changes in alkalinity may exert potential implications for sensitive ecosystems such as cold-water corals and seep-associated benthic communities (Sen et al., 2018; Sert et al., 2025). Overall, methane-driven transformations can alter the composition of dissolved and particulate organic matter, influence nutrient dynamics, and modify microbial community structure (Damm et al., 2008; Greinert et al., 2015; Mau et al., 2013; Sert et al., 2020). Consequently, methane seeps have implications that extend beyond local emissions, affecting ecosystem functioning at the water-column scale.

To assess the role of methane enrichment in the Arctic water column biogeochemistry, we utilise data collected across 28 research cruises conducted under the umbrella of CAGE (Centre of Excellence for Arctic Gas Hydrate, Environment, and Climate), hosted by UiT – The Arctic University of Norway. We compile, integrate and discuss methane and nutrient concentrations, hydrodynamic profiles, and organic carbon content, providing evidence for a highly dynamic Arctic methane biogeochemistry linked to methane release from the seabed and overlying water masses.

## 2 Methods

### 2.1 Study sites

A total of 68 multidisciplinary research cruises were conducted during CAGE's operational period (2013–2022). Of these, 28 cruises collected water-column methane concentration data, which were compiled and analysed in this study (Table 1). The water-column stations included in this study were grouped into six main hydrographic regions, each characterised by relatively consistent water-mass structure and circulation patterns (Fig. 1a-b). The deepest sampling was conducted along the Northern Mid-Atlantic Ridge (1), where water-column depths reached approximately 5000 m. The North Svalbard (2) region represents the northernmost coastal area and is primarily characterised by Arctic-type coastal waters. The West Svalbard (3) margin constitutes one of the most dynamic regions, where Atlantic Water and coastal water masses interact. This region also hosts one of the highest densities of documented methane seepage sites within the study areas. The Barents Sea is subdivided into two hydrographic regions. The Western Barents Sea (4) includes the major Atlantic inflow pathways through the submarine canyons Storfjordrenna and Bjørnøyrenna. In contrast, the Eastern Barents Sea (5) sites are more strongly influenced by Arctic water masses and relatively shallow water columns. Finally, northern Norway was investigated in the Lofoten–Vesterålen (6) region, where multiple cruises examined methane dynamics influenced by Atlantic inflow along the continental margin.

https://doi.org/10.5194/egusphere-2026-3607
Preprint. Discussion started: 30 June 2026


**Table 1. Overview of cruise dates, surveyed regions, and number of stations. HH, KPH, and GOS are the research vessels R/V Helmer Hanssen, R/V Kronprins Haakon, and R/V G.O. Sars, respectively.**

| | Cruise | R/V | Date | # | Visited areas |
|---|---|---|---|---|---|
| 1 | CAGE14-1 | HH* | 19 - 30 June 2014 | 91 | Prins Karls Forland (PKF)[1] |
| 2 | CAGE14-2 | HH | 01 - 06 July 2014 | 8 | PKF- Svyatogor |
| 3 | CAGE14-3 | HH | 07 - 21 July 2014 | 13 | Storfjordrenna - Crater area[2] |
| 4 | CAGE14-4 | HH | 21 - 29 July 2014 | 10 | Vestnesa- Storfjordrenna- Bjørnøyrenna[3] |
| 5 | CAGE15-3 | HH* | 27 Jun - 06 July 2015 | 65 | PKF[4] |
| 6 | CAGE15-5 | HH | 11 - 23 July 2015 | 20 | Crater area[5] |
| 7 | CAGE15-6 | HH | 07 - 27 Oct 2015 | 46 | Vestnesa- Svyatogor- PKF-Knipovich- Storfjordrenna[6] |
| 8 | CAGE16-2 | HH | 15 - 22 Apr. 2016 | 10 | Crater area- Bjørnøyrenna[7] |
| 9 | CAGE16-4 | HH* | 01 -09 May 2016 | 76 | PKF – Isfjorden[8] |
| 10 | CAGE16-5 | HH | 16 Jun - 4 July 2016 | 62 | PKF- Isfjorden- Storfjordrenna- Crater area[9] |
| 11 | CAGE16-7 | HH | 16 - 25 Oct 2016 | 19 | PKF- Crater area[10] |
| 12 | CAGE17-1 | HH* | 15 May - 02 June 2017 | 72 | Yermak Plateau- Vestnesa- PKF- Storfjordrenna[11-12] |
| 13 | CAGE17-2 | HH* | 21 June - 03 July 2017 | 15 | Storfjordrenna – Olga Basin[13] |
| 14 | CAGE17-3 | HH | 06 - 25 July 2017 | 5 | Crater area[14] |
| 15 | CAGE17-4 | HH | 03 - 06 Aug 2017 | 16 | KPF[15] |
| 16 | CAGE18-1 | HH | 12 - 20 May 2018 | 4 | Olga Basin[16] |
| 17 | CAGE18-2 | HH | 20 - 27 May 2018 | 15 | Lofoten – Vesterålen[17] |
| 18 | CAGE18-4 | HH | 19 Jul - 07 Aug 2018 | 16 | Molloy Deep – Bjørnøyrenna[18] |
| 19 | CAGE18-5 | KPH | 22 Oct - 02 Nov 2018 | 13 | Storfjordrenna – Olga Basin[19] |
| 20 | CAGE19-2 | HH | 09-23 July 2019 | 4 | PKF[20] |
| 21 | HACON19 | KPH* | 19 Sep- 16 Oct 2019 | 10 | PKF- Yermak Plateau- Gakkel Ridge- NE Svalbard[21] |
| 22 | CAGE20-1 | HH | 22 June - 01 July 2020 | 33 | PKF -Storfjordrenna[22] |
| 23 | CAGE20-7 | KPH | 02 - 16 Nov 2020 | 37 | PKF- Norskebanken – Hinlopen[23] |
| 24 | CAGE21-4 | HH | 02- 13 Aug 2021 | 8 | Hopendjupet[24] |
| 25 | HACON21 | KPH* | 28 Sep - 21 Oct 2021 | 5 | Molloy Deep – Gakkel Ridge[25] |
| 26 | CAGE21-6 | GOS | 05- 16 December 2021 | 43 | Hopendjupet[26] |
| 27 | CAGE22-3 | KPH* | 08- 16 June 2020 | 12 | Lofoten – Vesterålen[27] |
| 28 | CAGE22-6 | HH | 03- 20 Aug 2022 | 14 | Storfjordrenna - Hopendjupet – Bjørnøyrenna[28] |

Cruise reports for each campaign compiled here are publicly available via cited references ([2,5,7]Andreassen, 2014, 2015, 2016; [20]Andreassen et al., 2019; [14,18]Bünz, 2017, 2018; [19,21]Bünz et al., 2018, 2020; [1]Bünz and Panieri, 2014; [25]Bünz and Ramirez-Llodra, 2021; [9]Carroll, 2016; [8,10]Ferré et al., 2016a, b; [15,17]Ferré, 2017, 2018; [22,23,27]Ferré et al., 2020a, b, 2022; [6]Mienert et al., 2015; [13]Panieri et al., 2017b; [16]Plaza-Faverola, 2018; [4,11-12]Rasmussen et al., 2014, 2017a, b; [28]Serov et al., 2022; [4]Silyakova et al., 2015; [24]Winsborrow et al., 2021; [26]Winsborrow and Knies, 2021). *Data from these cruises have been published previously.

### 2.2 Water sampling and storage

Sampling areas were first investigated using hydroacoustic mapping of the seabed and water column. These surveys employed single-beam and/or multibeam echosounder systems (EK60/EK80 and EM300/EM302, respectively) to identify and map active

https://doi.org/10.5194/egusphere-2026-3607
Preprint. Discussion started: 30 June 2026


seepage sites. Water samples were collected using a rosette system equipped with Niskin bottles. Sensor-based profiling of the water column was conducted with a CTD (conductivity–temperature–depth) profiler (Sea-Bird SBE 911 plus) and an oxygen sensor (SBE 43). During each sampling occasion, water for methane concentration was collected immediately after the rosette was brought on board. Methane samples were collected in 120 mL serum bottles, amended with 1 mL of 1 M sodium hydroxide (NaOH), and sealed with butyl rubber septa using aluminium crimps. Samples were shaken vigorously and stored at 4 °C. At least 24 h prior to analysis, 5 mL of seawater was replaced with 5 mL of ultra-pure nitrogen to create a headspace for gas analysis (Magen et al., 2014). Methane oxidation (MOx) rate samples were collected, during selected sampling cruises, bubble-free into 20 mL glass vials sealed with bromobutyl rubber septa (Niemann et al., 2015). Samples for dissolved organic carbon (DOC), total dissolved nitrogen (TDN), particulate matter, and chlorophyll *a* (Chl *a*) were collected in acid-washed (2% HCl) glass bottles (4 × 1000 mL) and stored at 4 °C in the dark until processing. All samples were filtered within 6 h of collection using low-pressure vacuum filtration (≤ 50 mmHg). Triplicate samples for particulate matter and Chl *a* were collected on pre-combusted GF/F filters (Whatman) using 1 L of seawater per sample. Particulate matter filters were dried and stored at 25 °C until X-ray fluorescence analysis. Chl *a* filters were folded, placed in 10 mL high-density polyethylene (HDPE) tubes, and stored at -80 °C until analysis. Samples for nutrient analyses were collected in 40 mL HDPE bottles and stored at -20 °C until analysis.

### 2.3 Biochemical analyses

Methane samples were analysed using the headspace equilibration method (Magen et al., 2014) by gas chromatography (Thermo Scientific, GC Trace 1,310, FID detector, MSieve 5A column). MOx rates were determined using ex situ incubations with trace amounts of $^{3}H$-labelled $CH_4$, as previously described (Niemann et al., 2015; Steinle et al., 2015). Nitrate, silicate, and phosphate concentrations were measured colourimetrically using a segmented flow nutrient analyser (ALPKEM Flow Solution IV, OI Analytical) with detection limits of 0.5 µM, 0.06 µM and 0.4 µM (Grasshoff et al., 1999) and precisions of 0.1 µM, 0.1 µM and 0.01 µM, respectively. DOC and TDN concentrations were measured using a high-temperature combustion method (MQ Scientific MQ-1001) against in-house calibration standards and reference deep ocean samples (Qian and Mopper, 1996). $\delta^{18}O$ $H_2O$ was measured using a Thermo Scientific MAT253 isotope ratio mass spectrometry (IRMS). Isotopic ratios are reported relative to Vienna Standard Mean Ocean Water (VSMOW). International isotope standards VSMOW2, GISP (Greenland ice sheet precipitation), SLAP2 (Standard Light Antarctic Precipitation 2), and VPDB were used for the calibration of the IRMS with an uncertainty of < 0.01 ‰.

https://doi.org/10.5194/egusphere-2026-3607
Preprint. Discussion started: 30 June 2026


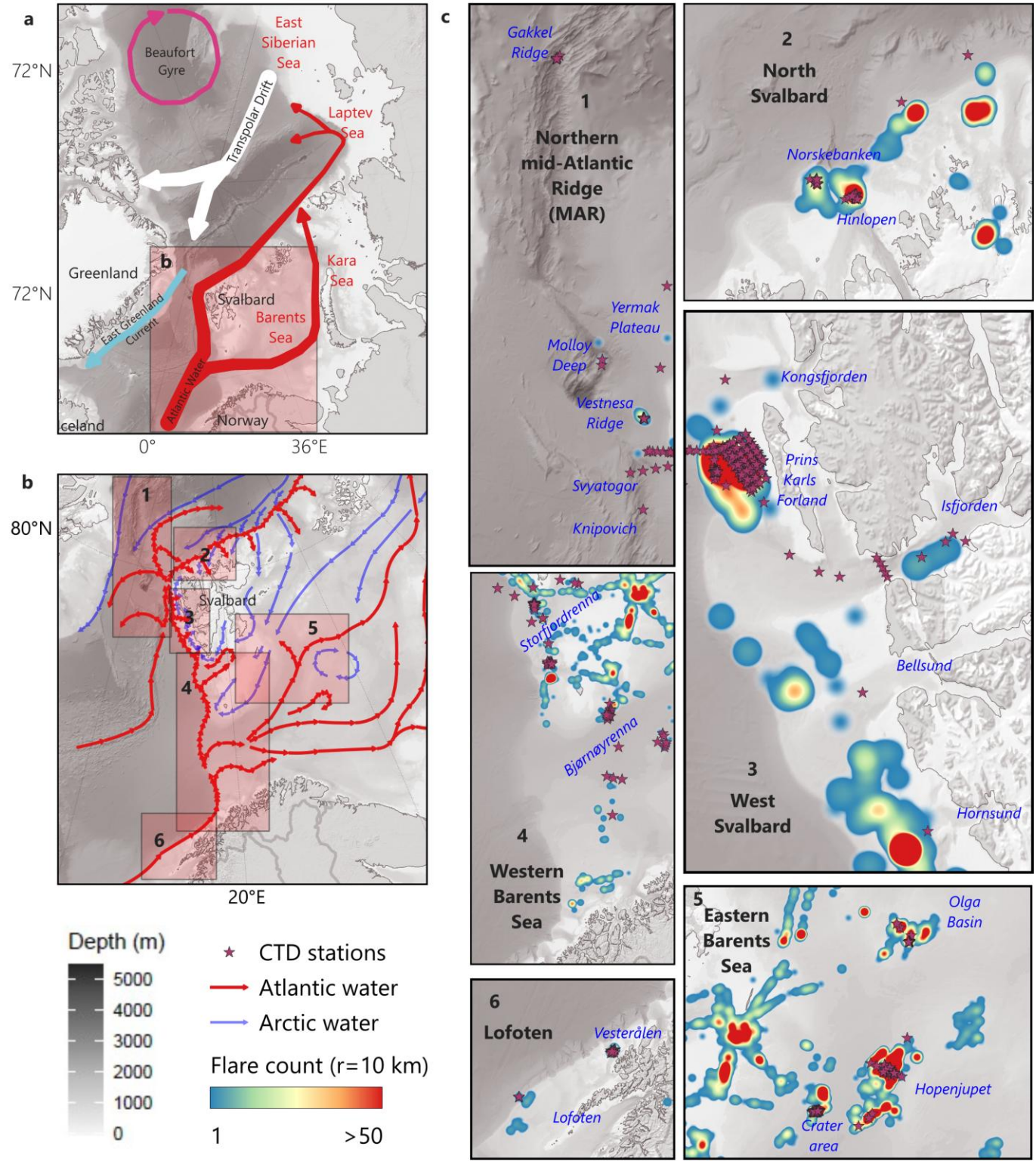

https://doi.org/10.5194/egusphere-2026-3607
Preprint. Discussion started: 30 June 2026


**Figure 1. (a) Overview map of the Arctic Ocean showing the study sites and large-scale circulation pathways. The shaded rectangle indicates the spatial extent of the inset shown in panel b. (b) Detailed ocean currents across the study site, with red arrows denoting the inflow of warm Atlantic Water and blue arrows indicating Arctic Water (Eriksen et al., 2018; Vihtakari, 2023). Shaded rectangles indicate the boundaries of the high-resolution sub-figures in panel c. (c) Detailed inset maps of the sampled study regions showing sampled stations (purple stars). Methane seeps are displayed as a heatmap generated via kernel density estimation using a radius of 10 km. Bathymetry is derived from the IBCAO grid (Jakobsson et al., 2012).**

### 2.4 Data acquisition

On all cruises, CTD profiling was conducted as a standard procedure to characterise the physical structure of the water column, even when the primary focus of the cruise did not directly involve water-column processes. Consequently, a comprehensive CTD dataset is available from all cruises. In the present study, however, we used only CTD data from stations where water sampling was performed. The complete CTD dataset can be found in the cruise reports (CAGE – Centre for Arctic Gas Hydrate, Environment and Climate Report Series, 2026) and adaptive cruise maps (CAGE's interactive geodata web map, 2026).

Some of the data compiled here (CTD, methane, methane oxidation rates, and nutrients) have been reported previously (Ferré et al., 2020, 2024; Gründger et al., 2021; Sert et al., 2020, 2022, 2023, 2025; Silyakova et al., 2015). In this study, these data are revisited and combined to provide a more comprehensive assessment of the study areas.

Active seep sites exhibited elevated methane concentrations in bottom waters, resulting in steep vertical gradients from highly supersaturated conditions (with respect to atmospheric pressure) near the seafloor to background levels in the overlying water column. Background methane concentrations were averaged from previously reported Atlantic Ocean methane concentrations (Keir et al., 2005; Kolomijeca et al., 2022; Scranton and Brewer, 1978). Several methane measurements fell below the headspace method's limit of detection (LOD) 0.74 nM (Magen et al., 2014). For these samples, methane concentrations were set to 0.52 nM, corresponding to LOD/√2 to substitute nondetectable values. Similarly, nutrient concentrations below the LOD (Grasshoff et al., 1999) were replaced with LOD/√2 (0.35 µM for nitrate, 0.04 µM for phosphate, and 0.28 µM for silicate) to account for nondetects. Dissolved organic nitrogen (DON) and dissolved organic phosphorus (DOP) concentrations were derived as the difference between total dissolved nitrogen and the sum of nitrate and ammonium, and between total dissolved phosphorus and phosphate, respectively. In some cases, total dissolved concentrations were measured lower than the sum of their constituents due to analytical uncertainties, resulting in negative calculated values. These negative values were removed before visualisation.

CTD data exhibiting anomalously low values within the upper few meters of the water column were filtered by excluding measurements with salinity < 30 and density < 25 kg $m^{-3}$, to remove spurious surface artefacts.

Methane turnover times were calculated as the inverse of the methane oxidation rate constant ($k_{Mox}$, $d^{-1}$) and subsequently converted to years by dividing by 365.

A combined dataset of methane seeps (Ferré et al., 2020c, 2024; Geissler et al., 2016; Mau et al., 2017; Thornes et al., 2023; Winsborrow et al., in prep) was mapped using Kernel Density Estimation (KDE) in QGIS (Fig. 1c). The density surface was calculated using a quadratic kernel function with a fixed search radius of 10 km, normalising the point data into a continuous grid of flare counts.

https://doi.org/10.5194/egusphere-2026-3607
Preprint. Discussion started: 30 June 2026


## 3 Overview of the study sites

### 3.1 Ocean currents and water masses

In all studied regions (Fig. 1b), the hydrography is governed by the interaction of relatively warm, saline Atlantic Water (AW, S > 34.8 and T > 2 °C) from the Norwegian Sea (Aagaard et al., 1987), Arctic Water (ArW, S < 34.8 and T < 0°C) from the Barents Sea (Oziel et al., 2016; Schauer et al., 2004), terrestrial influence (river runoff, glacial melt) and atmospheric forcing (cooling/heating, precipitation).

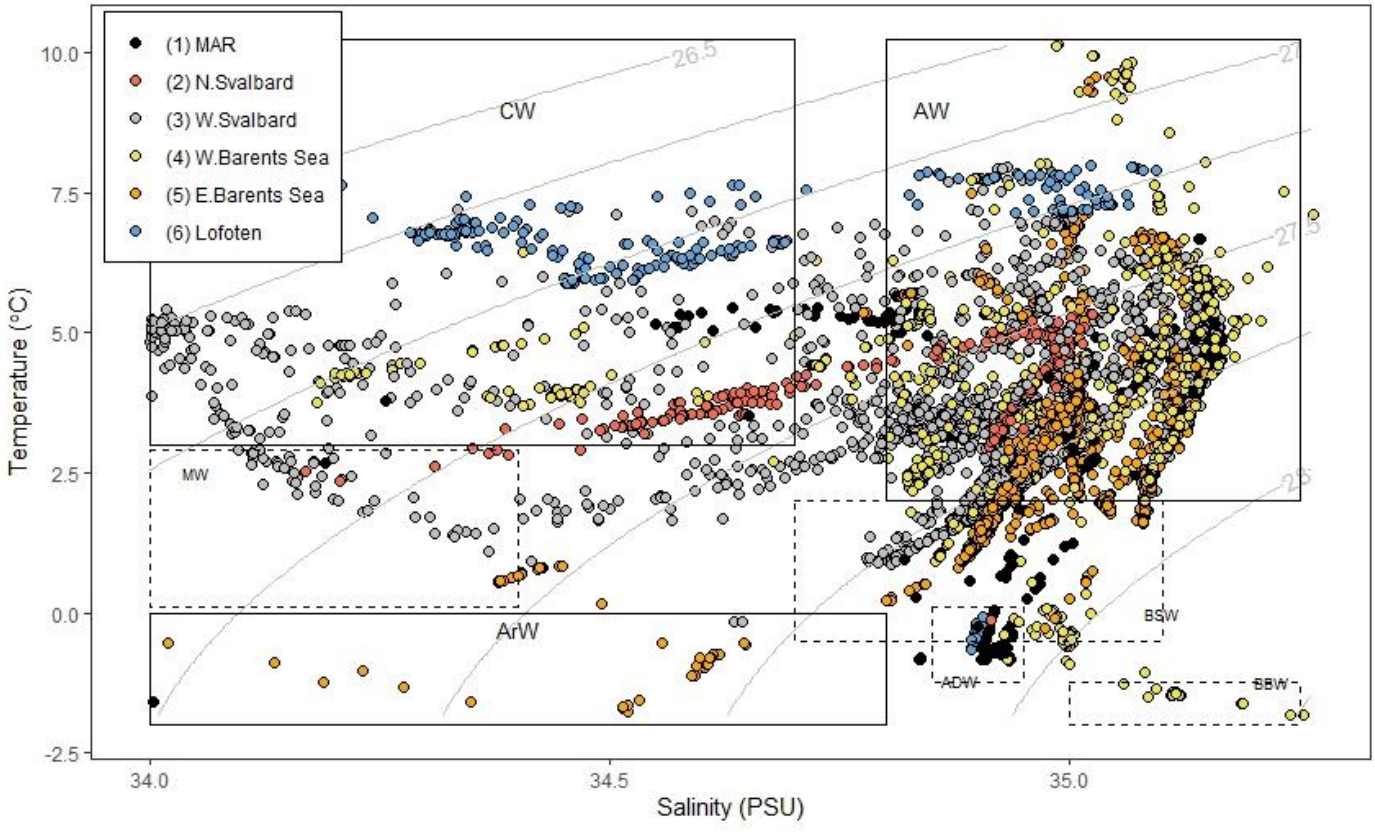


**Figure 2. Temperature–salinity (T–S) diagrams of all collected water samples. The three principal water masses, Atlantic Water (AW), Coastal Water (CW), and Arctic Water (ArW), are indicated by solid rectangles that represent their characteristic T–S domains. Locally formed or modified water masses, including Melt Water (MW), Barents Sea Water (BSW), Arctic Deep Water (ADW), and Barents Sea Bottom Water (BBW), are indicated by dashed rectangles. Coloured circles represent the sampling regions, as defined in Table 2 and Fig. 1c.**

West of Svalbard, the hydrography is governed by two northward-flowing current systems representing distinct water masses. The West Spitsbergen Current (WSC) and its eastern branch are topographically steered currents that primarily follow the shelf break and transport warm, saline AW into the region, strongly influencing the hydrography of the shelf break year-round (Aagaard et al., 1987). On the West Svalbard Shelf, a coastal current carries Coastal Water (CW, S < 34.7, T > 3 °C). This water mass originates from the Barents Sea via the Spitsbergen South Cape (Loeng, 1991), and is essentially cold, fresh ArW that is modified during its

https://doi.org/10.5194/egusphere-2026-3607
Preprint. Discussion started: 30 June 2026


northward flow along the coastline by river runoff, heating/cooling and mixing with other water masses. CW can therefore have a relatively wide range of properties depending on seasonal and interannual variability in forcing (Loeng, 1991; Oziel et al., 2016). Where and when AW penetrates onto the shelf, mixing can occur. These processes, i.e. interaction with the coastline and mixing between AW and CW, result in strong hydrographic variability, particularly at shallow locations (Nilsen et al., 2016). Despite the presence of these fresher water masses, the mean salinity across all sampled stations was around 34.9±0.5, indicating a predominance of AW and confirming the strong Atlantic influence on the hydrographic structure.

In the northern part of Svalbard, the regional circulation is dominated by the North Svalbard Current, a branch of the WSC that transports relatively warm AW (Fig. 1b) into the Arctic Ocean. After flowing around Northern Svalbard, AW follows the western margin of the trough mouth southward, partially recirculates over Norskebanken, and enters the Hinlopen Trough (Menze et al., 2020; Vanneste et al., 2006). In addition, the area is influenced by CW, which extends to depths of approximately 100 m and contributes to enhanced vertical stratification and heat transfer to the upper water column (Ferré et al., 2020b).

Water mass exchange between the Norwegian Sea and the Barents Sea is restricted by the relatively shallow average depth of the Barents Sea (~ 230 m). Deeper AW enters through two major pathways, i.e. Storfjordrenna and Bjørnøyrenna, where depths reach ~500 m (Loeng, 1991; Skogseth et al., 2005), while extensive shallow regions are found towards the Olga Basin (Fig. 1b). Consequently, only a limited fraction of AW penetrates into the Barents Sea, while the main branch continues northward through the Fram Strait as the WSC (Loeng, 1991; Schauer et al., 2004). AW inflow interacts with locally derived water masses through multiple mixing mechanisms, including entrainment, shear-induced turbulence, and mixing processes along frontal structures between colder arctic water masses and AW (Fer et al., 2003). This interaction plays a critical role in regulating the thermal structure, stratification, and overall hydrographic dynamics of the Barents Sea.

In addition to AW, ArW, and CW, several other characteristic water masses are present in the regions, including Meltwater (MW; S: 34-34.4, T:0-3 °C), Barents Sea Water (BSW; S: 34.7-35.1, T:-0.5-2 °C), Arctic Deep Water (ADW; S: 34.85-34.95, T:-1.25-0 °C), and Barents Sea Bottom Water (BBW: S: 35-35.25, T:-2--1.25°C) (Fig. 2). MW forms from sea-ice melt and glacial discharge, resulting in low-salinity surface layers that enhance upper-ocean stratification (Skogseth et al., 2005). BSW is formed through the transformation of AW within the Barents Sea via heat loss, brine rejection, and mixing processes. ADW originates in the Arctic Ocean and is characterised by cold, dense conditions at depth (Marnela et al., 2008), whereas BBW may form locally through winter cooling and brine-enriched convection, leading to the accumulation of dense bottom water (Oziel et al., 2016). These water masses are typically confined to areas with weak circulation and limited exchange, where local formation processes and seasonal variability exert strong control over hydrographic structure.

### 3.2 Geological settings of the study areas

#### 3.2.1 Svalbard margins and northern Mid-Atlantic Ridge (Regions 1, 2, and 3)

The West Svalbard continental margin (<500 m water depth) off Prins Karls Forland (PKF) Island was the most visited site (Table 1). The continental shelf (i.e., water depth <100 m) is characterised by hundreds of gas flares and elevated methane concentrations

https://doi.org/10.5194/egusphere-2026-3607
Preprint. Discussion started: 30 June 2026


throughout the water column, sometimes reaching the sea surface, indicating potential atmospheric fluxes from the shallow water column (Steinle et al., 2015). At the continental slope (300 m), seepage activity dates back 8000 years (Berndt et al., 2014), and the boundary depth of the GHSZ varies from 360 to 410 m, depending on bottom-water temperatures (Ferré et al., 2020c).

The investigated sites extend into deeper environments (> 500 m depth) along the western Svalbard continental margin and towards the northern Mid-Atlantic Ridge (MAR). These sites include the Knipovich Ridge, Svyatogor Ridge, Vestnesa Ridge, Molloy Deep, Yermak Plateau, and Gakkel Ridge (Fig. 1a). Northward, the MAR transitions from a classical oceanic spreading ridge into a complex system of ultraslow-spreading ridges extending into the Arctic Ocean (DeMets et al., 2010). This tectonic setting extends to the ultraslow-spreading Gakkel Ridge and influences the development of contourite drifts and sedimentary depositional patterns such as Vestnesa Ridge, Svyatogor Ridge and the Yermak Plateau. Vestnesa Ridge is one of the most intensively studied areas due to its prominent pockmark field and active gas flares (Fig. 1c), which represent major conduits for methane seepage (Bünz et al., 2012; Johnson et al., 2015; Panieri et al., 2017a; Portnov et al., 2016; Sauer et al., 2020; Schneider et al., 2018; Smith et al., 2014; Sztybor and Rasmussen, 2017; Yao et al., 2019). Seismic and hydroacoustic observations document persistent methane release from subsurface reservoirs, with gas flares rising through the water column (Bünz et al., 2012; Panieri et al., 2017a; Sztybor and Rasmussen, 2017). The pockmarks are rich in methane-derived authigenic carbonates and host diverse chemosynthetic fauna, indicating long-term seep activity (Åström et al., 2018; Dessandier et al., 2019; Sztybor and Rasmussen, 2017; Yao et al., 2021). The northern MAR region is characterised by intense faulting and rifting, associated with high heat flow.

As the final pathway for warm Atlantic water entering the Arctic Ocean, the Yermak Plateau serves as a significant topographic barrier (Fig. 1a) that influences the circulation and transformation of the Atlantic inflow (Fer et al., 2015). The plateau also hosts the northern Svalbard marginal ice zone, a dynamic interface between the open ocean and sea ice (Rudels et al., 2005). This region contains one of the largest known submarine landslides, the Hinlopen slide (Vanneste et al., 2006; Winkelmann and Stein, 2007), which has transported substantial volumes of sediment from this Arctic continental margin into the Nansen Basin, thereby playing an important role in shaping the Arctic seafloor morphology and sedimentary processes (Vanneste et al., 2006; Winkelmann et al., 2006).

The Hinlopen Slide occurred at the mouth of the Hinlopen Trough about 30,000 years ago during the Late Pleistocene, likely a period of rapid glaciogenic sediment accumulation and rapid sea-level lowering (Geissler et al., 2016). During this event, 200 $km^3$ of sediment were remobilised, exposing gas hydrate deposits a few kilometres to the north, as well as widespread free gas accumulations and active seeps (Fig. 1c) within and adjacent to the slide area (Geissler et al., 2016; Vanneste et al., 2006). Previous observations reported water-column methane concentrations of up to 218 nM, indicating substantial seafloor methane release (Geissler et al., 2016). Moreover, elevated atmospheric methane concentrations at 80°N, 12°E suggest an ocean–atmosphere methane flux that cannot be explained by wetlands or known anthropogenic sources, pointing instead to a marine contribution (Platt, 2015).

https://doi.org/10.5194/egusphere-2026-3607
Preprint. Discussion started: 30 June 2026


### 3.2.2 Western Barents Sea (Region 4)

The dissolution of gas hydrates and methane ebullition from the seabed are key processes that contribute to the formation of distinct geomorphological features in marine sediments and on the seafloor due to fluid flow (e.g., Judd and Hovland, 2007; Mienert et al., 2022). Features such as craters, pockmarks, and pingo-like structures are widespread on Arctic shelves and in the Barents Sea, reflecting episodic methane release events over geological timescales. The northernmost cross-shelf area of Storfjordrenna hosts seven gas-hydrate pingos that actively emit free gas into the water column (Carroll, 2016). These pingos contain methane-derived authigenic carbonates and support exceptionally rich benthic fauna at water depths of approximately 350–390 m, corresponding to the gas hydrate stability zone and its upper termination (Sen et al., 2018). Variability in water-column temperature, driven by the inflow of warm AW via the WSC, its mixing with colder ArW, and episodic brine outflows from Storfjorden (Fer et al., 2003), modulates gas-hydrate stability and controls methane-release dynamics in the area.

### 3.2.3 Eastern Barents Sea (Region 5)

The crater areas are among the most intensively studied and are characterised by kilometre-wide depressions formed by methane blowouts associated with rapid gas hydrate destabilisation during the last deglaciation, approximately 15,000 years before present (Andreassen et al., 2017; Portnov et al., 2013, 2014; Serov et al., 2015). Although these large-scale blowout events occurred in the past, the associated structures continue to emit methane at lower and more stable rates. For example, Barents Sea craters are irregularly distributed across an area of approximately 500 km² at water depths of 310–360 m, with individual depressions reaching 5–30 m in depth (Carroll, 2016).

Hopendjupet (Fig. 1c) also hosts an extensive crater field with strong gas flaring linked to thermogenic source rocks. Gas hydrate stability in this area occurs at approximately 360 m water depth (Patton et al., 2020; Serov et al., 2022). Major regional geological structures serve as focal points for the migration of free gas from the subsurface (Serov et al., 2024). Cruises in the area have documented extremely intense gas seepage, presence of gas-hydrate pingos, and oil slicks at the sea surface, highlighting the ongoing activity of methane release and associated hydrocarbon fluxes (Winsborrow et al., 2021; Winsborrow and Knies, 2021) .

In the northern section of Hopendjupet, Olga Basin is the easternmost site studied and provides insight into the hydrodynamics of the north-central Barents Sea. This area also hosts craters in the southern part of Storbanken, which are associated with several gas flares, carbonate crusts, and bacterial mats, features that have been extensively investigated during multiple cruises (Table 1). Water depths in this region are approximately 150 m, and the craters often exhibit very steep slopes, highlighting the localised geomorphological impact of Jurassic-age outcrops (Bünz et al., 2018).

### 3.2.4 Lofoten-Vesterålen (Region 6)

The southernmost region investigated during the CAGE expeditions is Lofoten–Vesterålen, located along the Mid-Norwegian continental margin. Methane seepage dynamics in this region differ from those observed at the margins of Svalbard and the Barents Sea, primarily due to lower methane concentrations, weaker flare activity, and enhanced vertical and turbulent mixing in the water

https://doi.org/10.5194/egusphere-2026-3607
Preprint. Discussion started: 30 June 2026


column (Ferré et al., 2024). Seepage activity is spatially heterogeneous and linked to shallow gas accumulations and structurally controlled fluid migration pathways (Ferré et al., 2024). Geochemical analyses indicate that the emitted methane is primarily of thermogenic origin (Sauer et al., 2015), while dating of methane-derived authigenic carbonate crusts suggests that seepage has been active for at least ~11 kyr (Chand et al., 2008; Crémière et al., 2016). These carbonate structures commonly support microbial mats and tubeworm assemblages typical of Arctic seep ecosystems (e.g. Argentino et al., 2022). The Hola Trough also hosts abundant cold-water coral communities, including *Desmophyllum pertusum (Lophelia pertusa),* forming a unique benthic ecosystem (Rastrick et al., 2018; Sert et al., 2025). Here, sedimentary inputs modulate the physicochemical properties of the overlying water column and contribute to reef development via carbonate chimneys, which provide structural habitats that sustain coral growth and associated biodiversity (Argentino et al., 2025).

## 4 Results

### 4.1 Ocean temperature, salinity, density and oxygen

Among all regions, the highest average temperatures throughout the water column were recorded off Lofoten-Vesterålen. Here, the AW showed an average temperature of 6.4 °C, with a range of −0.7 to 8.0 °C (Table 2). In contrast, the northern MAR showed the lowest average temperatures, with a mean of 2.1 °C, ranging from −1.8 to 6.7 °C. Across all study regions, temperatures ranged from −1.8 to 10.1 °C, reflecting seasonal variability and differences in water-mass characteristics (Table 2).

The highest average salinity was observed in the Eastern Barents Sea (34.95), followed closely by the Western Barents Sea (34.93) and West Svalbard (34.89), while the lowest mean occurred off Lofoten (34.64). Salinity ranges varied substantially, particularly in coastal areas and at PKF, indicating an episodic influx of less saline coastal waters. Across all regions, salinity ranged from 31.61 to 35.26 (Table 2).

The highest mean density was at deep Northern Atlantic waters (27.85 kg $m^{-3}$) and the Eastern Barents Sea (27.83 kg $m^{-3}$), whereas the lowest occurred off Lofoten (27.19 kg $m^{-3}$), reflecting the higher temperature and lower salinity in this region. Density varied in broader ranges in regions affected by surface waters from meltwater runoff.

Dissolved oxygen showed moderate variability between study areas. The highest mean concentration was measured north of Svalbard (6.90 mL $L^{-1}$), while the lowest was observed at Northern MAR (5.99 mL $L^{-1}$). Across all regions, oxygen concentrations ranged from 4.72 to 10.14 mL $L^{-1}$ (Table 2).

Mean $\delta^{18}O$ values reached 0.33‰ (0.24–0.41‰) in the Eastern Barents Sea, 0.13‰ (−2.34–0.48‰) at the Northern MAR, 0.37‰ (0.01–0.68‰) at West Svalbard, and 0.40‰ (0.18–0.65‰) in the Western Barents Sea (Table 2). Overall, $\delta^{18}O$ values exhibited a relatively narrow range and were predominantly positive, indicating Atlantic-dominated water masses. Negative values were observed only in the upper water column at the Gakkel Ridge (Fig. 3), suggesting the influence of Pacific seawater or isotopically depleted meteoric water, potentially derived from snowmelt or riverine input characterised by negative $\delta^{18}O$ composition (Alkire et al., 2010, 2007). All other measurements showed positive, relatively enriched $\delta^{18}O$ values, ranging from 0.01 to 0.68‰.

https://doi.org/10.5194/egusphere-2026-3607
Preprint. Discussion started: 30 June 2026


**Table 2. Physical and biogeochemical measurements obtained from CTD casts and Niskin bottle samples. All measured parameters are grouped by the six main hydrographic areas (Fig. 1c). For each parameter, the regional mean value is reported, along with the whole range in brackets.**

| Site | (1) Northern MAR | (2) North Svalbard | (3) West Svalbard | (4) Western Barents Sea | (5) Eastern Barents Sea | (6) Lofoten |
|---|---|---|---|---|---|---|
| # sampling points | 361 | 257 | 3179 | 885 | 1148 | 248 |
| Max. depth (m) | 4098 | 856 | 483 | 1488 | 361 | 800 |
| Temp. (°C) | 2.13 [-1.76 - 6.67] | 4.08 [-0.13 - 5.32] | 3.50 [-0.16 - 7.98] | 3.73 [-1.83 - 10.14] | 2.93 [-1.75 - 9.57] | 6.44 [-0.66 - 7.98] |
| Salinity | 34.82 [31.61 - 35.17] | 34.82 [34.17 - 35.02] | 34.89 [33.41 - 35.16] | 34.93 [32.36 - 35.26] | 34.95 [33.78 - 35.15] | 34.64 [33.98 - 35.09] |
| Density (kg $m^{-3}$) | 27.85 [25.42 - 28.09] | 27.61 [23.56 - 28.05] | 27.74 [26.64 - 28.03] | 27.73 [25.64 - 28.39] | 27.83 [27.05 - 28.10] | 27.19 [26.51 - 28.05] |
| Oxygen (mL $L^{-1}$) | 5.99 [5.39 - 9.60] | 6.90 [6.14 - 8.11] | 6.41 [4.72 - 10.14] | 6.71 [5.32 - 8.83] | 6.44 [4.98 - 9.79] | 6.54 [6.22 - 8.16] |
| Methane (nM) | 40.82 [0.52 - 5982] | 45.50 [0.78 - 4461] | 47.68 [0.52 - 739] | 908 [0.52 - 220014] | 113.92 [0.52 - 50655] | 17.46 [0.79 - 447.71] |
| MOx (nM $day^{-1}$) | - | - | 0.07 [0.00 - 7.07] | 0.10 [0.00 - 0.95] | 3.34 [0.00 - 31.59] | |
| Nitrate (µM) | 10.52 [0.35 - 15.83] | 9.71 [5.83 - 12.25] | 8.18 [0.35 - 12.70] | 7.81 [0.35 - 14.91] | 8.77 [0.35 - 11.74] | 8.17 [0.35 - 11.36] |
| Phosphate (µM) | 0.87 [0.26 - 1.27] | 0.67 [0.46 - 0.84] | 0.69 [0.06 - 1.39] | 0.76 [0.12 - 1.94] | 0.75 [0.04 - 1.57] | 0.58 [0.15 - 1.08] |
| Silicate (µM) | 7.12 [2.61 - 13.29] | 4.09 [2.44 - 6.23] | 3.91 [0.70 - 13.56] | 4.26 [0.70 - 13.54] | 4.07 [0.54 - 7.44] | 4.08 [1.68 - 5.33] |
| DOC (µM) | 50.70 [26.92 - 91.96] | 56.08 [37.70 - 63.90] | 63.54 [37.34 - 102.84] | 48.45 [32.75 - 68.49] | 57.56 [33.97 - 104.02] | 59.80 [52.00 - 71.30] |
| DON (µM) | 2.19 [0.00 - 14.96] | 3.32 [0.00 - 8.04] | 8.19 [2.05 - 14.07] | 5.17 [0.00 - 8.54] | 3.62 [0.00 - 15.39] | 3.65 [1.17 - 6.99] |
| DOP (µM) | 0.06 [0.00 - 0.15] | - | 0.13 [0.01 - 0.28] | 0.09 [0.00 - 0.19] | 0.14 [0.05 - 0.60] | - |
| Ammonium (µM) | 0.09 [0.01 - 0.32] | - | 0.92 [0.03 - 2.08] | 0.84 [0.18 - 6.21] | 0.71 [0.04 - 1.87] | - |
| PC (µM) | 1.71 [0.51 - 5.49] | - | 7.16 [1.85 - 16.84] | 6.87 [1.04 - 35.64] | 3.14 [2.39 - 5.02] | - |
| PN (µM) | 0.12 [0.00 - 0.60] | - | 0.74 [0.07 - 1.81] | 0.49 [0.00 - 1.93] | 0.35 [0.20 - 0.49] | - |
| PP (µM) | 0.03 [0.01 - 0.09] | - | 0.09 [0.03 - 0.21] | 0.06 [0.01 - 0.17] | 0.05 [0.04 - 0.07] | - |
| Chl-a (mg $L^{-1}$) | 0.28 [0.00 - 1.00] | - | 1.02 [0.36 - 2.73] | 0.83 [0.02 - 5.75] | 0.42 [0.04 - 0.92] | - |
| $\delta^{18}O$ (‰) | 0.13 [-2.34 - 0.48] | - | 0.37 [0.01 - 0.68] | 0.40 [0.18 - 0.65] | 0.33 [0.24 - 0.41] | - |

https://doi.org/10.5194/egusphere-2026-3607
Preprint. Discussion started: 30 June 2026


315

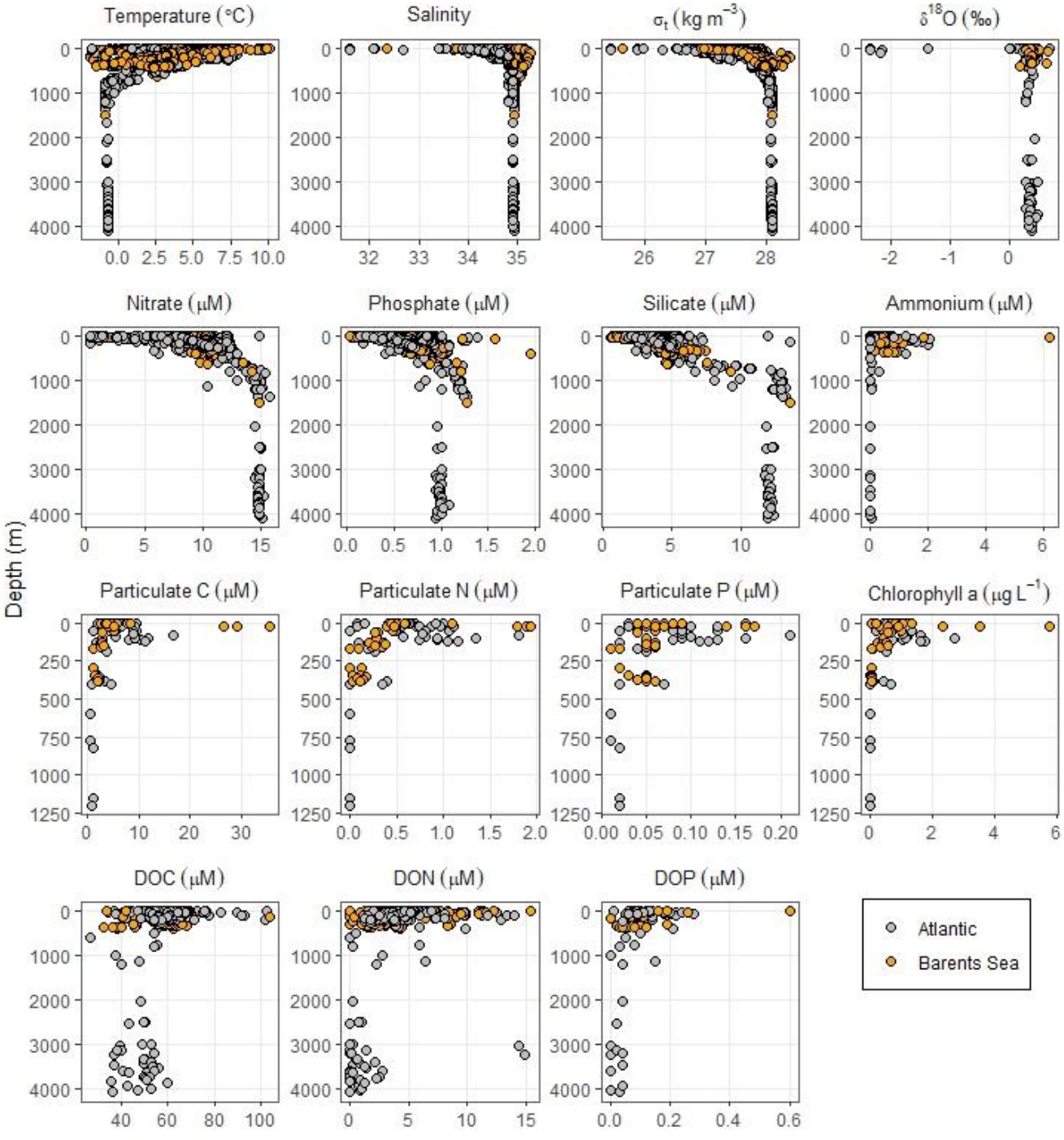

https://doi.org/10.5194/egusphere-2026-3607
Preprint. Discussion started: 30 June 2026


**Figure 3. Vertical distributions of biogeochemical parameters in the water column across all study regions. Sites predominantly influenced by Atlantic-origin waters (previously referred to as the (1) Northern Mid-Atlantic Ridge, (2) North Svalbard, (3) West Svalbard, and (6) Lofoten) are grouped as Atlantic. Eastern Barents Sea (4) and Western Barents Sea (5) sites are grouped together as the Barents Sea.**

### 4.2 Methane and MOx

Among all methane measurements, the highest concentrations were recorded at the gas-hydrate pingos in Storfjordrenna, Western Barents Sea (Table 2). These structures are associated with active fluid seepage (Waage et al., 2019) and were sampled during ROV dives, where methane concentrations reached up to 220,015 nM. Elevated concentrations were also measured in the Hinlopen region of the Barents Sea using ROV-based sampling (Winsborrow and Knies, 2021), with values reaching 50,655 nM. These near-seafloor ROV measurements substantially increased the regional mean methane concentrations compared to conventional CTD-rosette water-column sampling, yielding average values of 113 nM in the Eastern Barents Sea and 908 nM in the Western Barents Sea.

At West Svalbard, methane concentrations were consistently elevated in bottom samples with a mean concentration of 47.68 nM. The maximum value (739 nM) was recorded at 100 m water depth near a dense cluster of seeps. Across all 344 stations where methane was measured at water depths ranging from 59 to 419, the overall mean concentration was 49 nM. Mean methane concentrations were 40.82 nM at the MAR samples and 45.50 nM north of Svalbard, whereas the lowest concentrations were observed off Lofoten, with a mean concentration of 17.46 nM.

https://doi.org/10.5194/egusphere-2026-3607
Preprint. Discussion started: 30 June 2026


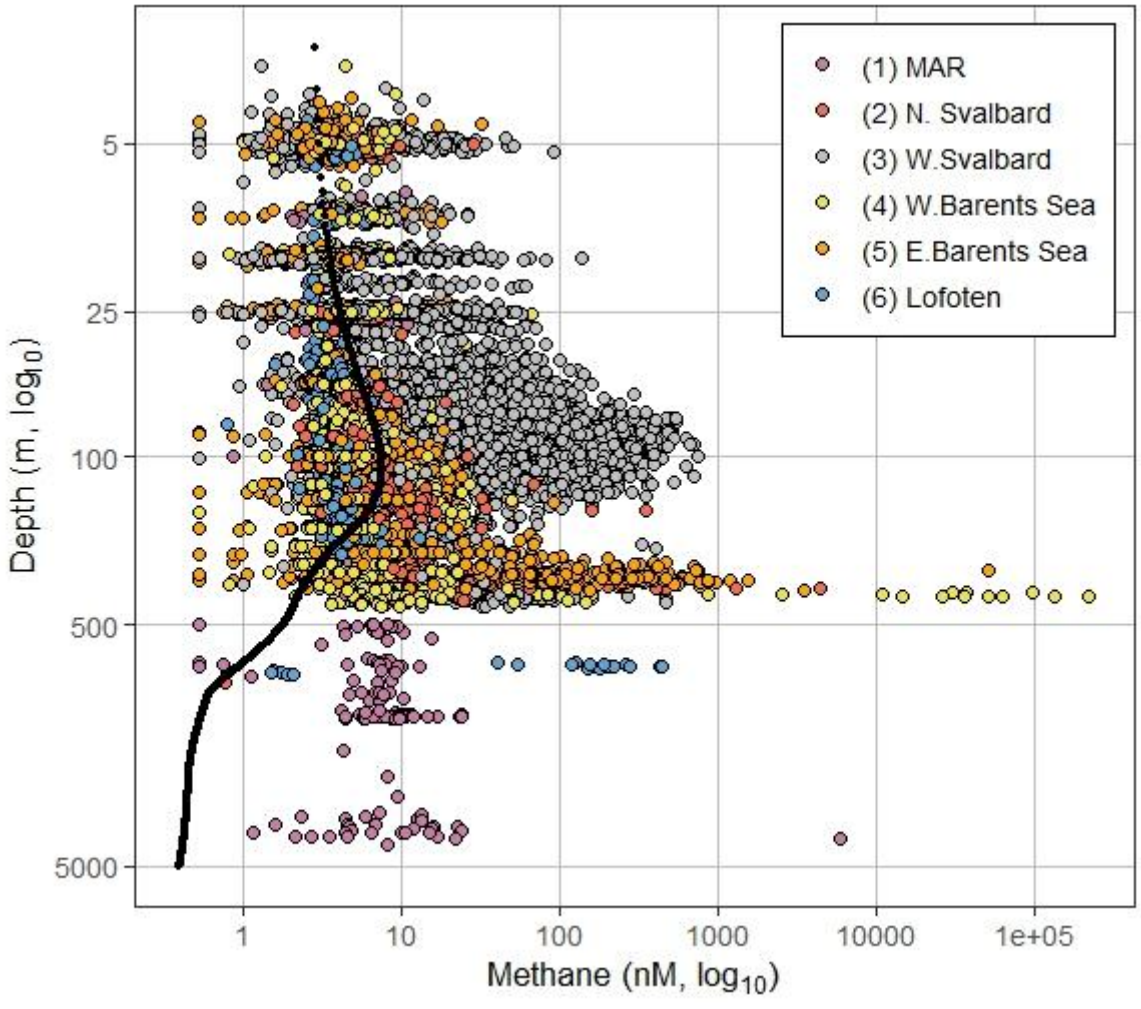


340

**Figure 4: Depth distribution of methane concentrations in water column samples across all study regions. Both axes are on a logarithmic scale. Colours indicate sampling regions: Eastern Barents Sea (orange), Western Barents Sea (pink), Lofoten (green), North Svalbard (purple), West Svalbard (grey), and Northern Mid-Atlantic Ridge (blue). The black dotted line represents the approximate background methane concentration profile averaged from previous Atlantic measurements (Keir et al., 2005; Kolomijeca et al., 2022; Scranton and Brewer, 1978).**

345

https://doi.org/10.5194/egusphere-2026-3607
Preprint. Discussion started: 30 June 2026


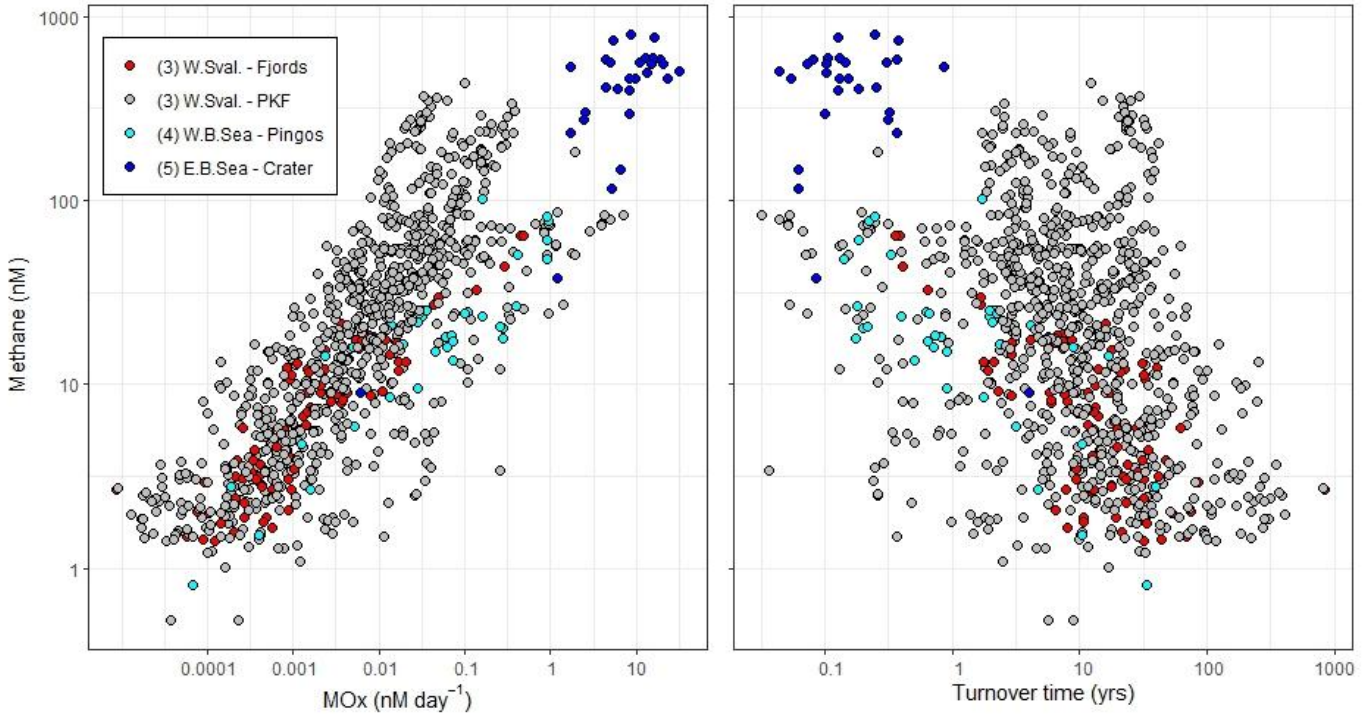


**Figure 5. Relationship between methane (nM) versus MOx (nM day$^{-1}$) and turnover time (years, yrs). All axes are presented on a $\log_{10}$ scale. Data points are colour-coded by study areas. Numerical prefixes in the legend correspond to the study regions given in Table 1 and Fig. 1c: (3) West Svalbard (including fjords and PKF sites), (4) Eastern Barents Sea (Pingos), and (5) Western Barents Sea (Crater area).**

The highest MOx was measured in the crater area of the Eastern Barents Sea (Table 2), reaching a maximum of 31.6 nM day$^{-1}$ at 500 m water depth near the seafloor. At PKF, West Svalbard, maximum MOx reached 7.07 nM day$^{-1}$, while at the pingo site in Storfjordrenna (Western Barents Sea), the maximum rate was 0.95 nM day$^{-1}$. Although MOx measurements were not conducted at all sites, when measured, detectable rates were generally confined to the lower part of the water column, where methane concentrations were highest. In contrast, MOx in the upper water column were typically negligible or below detection limits. A distinct regional contrast was evident among the study areas (Fig. 5). Methane oxidation appears to be more efficient in the Eastern Barents Sea than in West Svalbard. For example, MOx rates in the crater area of the Eastern Barents Sea were up to 250 times higher than those measured at West Svalbard (Table 2). Overall, MOx activity in the Eastern Barents Sea was approximately one to three orders of magnitude higher than in the Western Svalbard region. This contrast was also reflected in methane turnover times. In the crater area, turnover times were generally less than a year, whereas at PKF and in the Svalbard fjords, they ranged from 1 to 1,000 years (Fig. 5). The Pingo site in Storfjordrenna exhibited comparatively shorter turnover times than the PKF, ranging from months to 50 years (Fig. 5).

https://doi.org/10.5194/egusphere-2026-3607
Preprint. Discussion started: 30 June 2026


### 4.3 Nutrients

Inorganic nutrients were measured across all six regions, encompassing 184 stations and 1,466 sampling depths. The overall mean concentrations were 8.5 µM for nitrate, 0.72 µM for phosphate, and 4.41 µM for silicate. The concentration ranges are similar among regions and aligned with the observed hydrographic structure of the water column. Vertical distributions of nutrients followed characteristic water-mass stratification patterns, with nutrient enrichment occurring below the biologically productive surface layer (Fig. 3). Ammonium was measured during two cruises (CAGE 17-1 and CAGE 17-2), covering the Eastern and Western Barents Sea, PKF, and the Northern Mid-Atlantic Ridge. Except for a single elevated concentration of 6.21 µM at the surface at the pingo site, ammonium concentrations ranged from 0.01 to 2.08 µM. Ammonium did not exhibit a consistent depth-related pattern, yet concentrations were generally higher in the surface and subsurface layers.

DOC concentrations were highest in the surface layer, reaching 102 µM in PKF, 104 µM in the Olga basin, and 91 µM in the Gakkel Ridge (Fig. 3). DOC decreased rapidly with depth at most of the studied sites. Dissolved organic nitrogen (DON) was highly correlated with DOC and showed a similar pattern in all stations. DON concentrations ranged from 0 to 15.39 µM, with the highest measured in Olga Basin.

Particulate carbon (PC), particulate nitrogen (PN), particulate phosphorus (PP), and chlorophyll a (Chl-a) were measured during the CAGE17-1 and CAGE17-2 cruises at PKF, Olga Basin, Storfjordrenna, and Vestnesa Ridge. Associated with primary production, these parameters were consistently at their maximum in the surface and subsurface layers and rapidly fell below the detection limit at the nutricline (Fig. 3).

Stoichiometric relationships between nitrate and phosphate, and between nitrate and silicate, showed strong and consistent correlations, with R values of 0.90 and 0.77, respectively, indicating stable nutrient coupling across the sampled regions (Fig. 6). Compared to the canonical Redfield ratio (Redfield, 1958) (N:P = 16:1) and the typical marine N:Si relationship (~1:1 for diatom-dominated systems), the observed slopes suggest deviations from suggested stoichiometric proportions. In particular, the nitrate-to-phosphate ratio indicates relative nitrate limitation, while the nitrate-to-silicate ratio suggests silicate limitation relative to nitrate availability (Fig. 6).

https://doi.org/10.5194/egusphere-2026-3607
Preprint. Discussion started: 30 June 2026


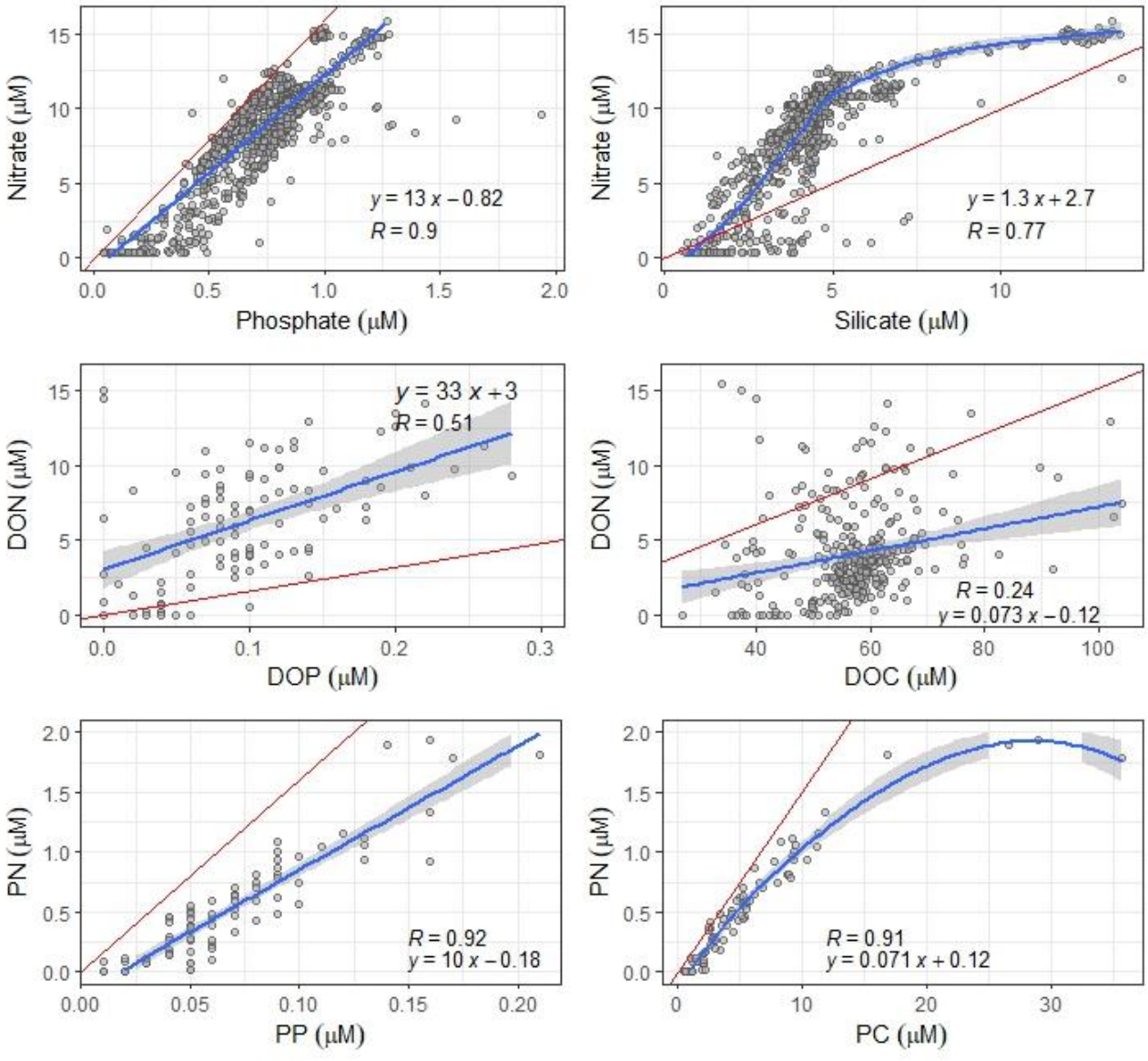


**Figure 6: Stoichiometric relationships between dissolved and particulate nutrients. Blue solid lines represent best-fit linear regressions or LOESS smoothing (with shaded standard error); red lines indicate the classical Redfield ratios (N:P = 16:1; C:N = 6.6:1). Linear regression equations and Pearson correlation coefficients (R) are provided within each panel. Abbreviations: dissolved/particulate organic carbon (DOC, PC), nitrogen (DON, PN), and phosphorus (DOP, PP).**

https://doi.org/10.5194/egusphere-2026-3607
Preprint. Discussion started: 30 June 2026


## 5 Discussion

### 5.1 Variability of methane and MOx in Arctic margins

Our results demonstrate pronounced regional variability in methane dynamics across Arctic seep systems (Fig. 4, Table 2). Although methane enrichment was generally confined to bottom waters near seep sites, the magnitude of methane accumulation and MOx differed markedly among regions. The strongest methane enrichment occurred in seep sites in the Barents Sea, particularly in the Pingo site, Hopendjupet, and the Crater area, where both methane concentrations and methane oxidation (MOx) rates substantially exceeded those observed along the West Svalbard margin (Fig. 4, Table 2). These differences likely reflect contrasts in seep intensity, hydrographic conditions, and geological settings among regions.

Localised high-intensity seep sites further highlight this variability. Pingos in the Storfjordrenna represent methane-release hotspots, where methane concentrations can reach orders of magnitude higher than those observed at most other Arctic seep systems. Under such extreme conditions, methane supply exceeds the capacity of local methanotrophic communities to oxidise methane, allowing a greater fraction to bypass the microbial filter and potentially reach the atmosphere.

Similar regional variability was evident in MOx rates and turnover times (Fig. 4). MOx rates in the Eastern Barents Sea were two to three orders of magnitude higher than those measured at the West Svalbard at similar methane concentrations. Similarly, microbial turnover times are orders of magnitude smaller in Crater area than in the PKF and West Svalbard Fjords, indicating substantially more efficient methane consumption. These findings indicate that methane oxidation is not solely controlled by methane availability but is also strongly influenced by regional environmental factors. Differences in hydrography, water-mass residence times, microbial community structure, and nutrient availability likely regulate methanotrophic activity and, consequently, the efficiency of methane removal from the water column.

In highly dynamic water columns, where mixing, advection, and drift continuously disturb the system, the establishment of a stable MOB community is less likely (Steinle et al., 2015). Under such conditions, even substantial methane inputs from seepage may not translate into elevated MOx rates because the microbial community cannot maintain sufficient abundance to efficiently consume methane. In contrast, under more stable hydrographic conditions, MOB communities can develop and persist, thereby making MOx a more effective methane sink (Steinle et al., 2015). Temporal mismatches between methane supply and microbial response may also occur, such that sudden increases in methane flux are not immediately accompanied by enhanced MOx activity because MOB populations cannot rapidly adjust in abundance. In addition, MOB also require micronutrients such as copper and iron, which are essential for methanotrophic enzymatic pathways (Hanson and Hanson, 1996). The availability of these micronutrients may therefore regulate the growth and activity of MOB communities and influence their capacity to buffer methane seep emissions.

### 5.2 Fate of methane in the water column

Following the first discoveries of extensive seep systems in the Arctic Ocean that release methane from the seabed into the overlying water column (Westbrook et al., 2009), significant scientific attention focused on whether methane released from melting gas hydrates on the seafloor could reach the atmosphere (Ruppel and Kessler, 2017), amplify climate warming and potentially

https://doi.org/10.5194/egusphere-2026-3607
Preprint. Discussion started: 30 June 2026


catastrophic climate feedback effects (Biastoch et al., 2011; James et al., 2016; Shakhova et al., 2010). Subsequent investigations and more detailed process-based studies, however, have provided a more nuanced understanding (Dølven et al., 2025; Ferré et al., 2020c; Joung et al., 2022; Myhre et al., 2016; Platt et al., 2018).

Although active seeps inject substantial amounts of methane into the water column, most methane often does not immediately reach the sea surface (Myhre et al., 2016). Bubbles (free gas) tend to dissolve rapidly and exchange gases with the surrounding seawater as they ascend (Jansson et al., 2019; Veloso-Alarcón et al., 2019). The efficiency of methane transport from seep sites to the atmosphere is further modulated by several physical factors, including water depth, bubble size, rise velocity, and the presence of hydrate or organic coatings that can stabilise bubbles and slow dissolution (Jansson et al., 2019; Marcon et al., 2025; McGinnis et al., 2006). In deeper waters, prolonged bubble ascent enhances dissolution and horizontal transport, thereby limiting direct atmospheric transfer.

Once dissolved, methane is oxidised by MOB and converted to carbon dioxide. This reduces atmospheric methane emissions, however, the effect is not well quantified. Measurements of atmospheric methane above seep areas generally support a local attenuation effect (McGinnis et al., 2006; Myhre et al., 2016), but the fate of the dissolved methane that leaves the local area via ocean currents is challenging to determine. In fact, recent methane fate modelling studies suggest that the dissolved methane (of bubble origin) that is laterally advected away from the local area is the dominant contributor to methane release from the ocean (Dølven et al., 2025; Nordam et al., 2025). This release of seep-origin dissolved methane can, however, be a relatively slow process (weeks to years) because it is transported laterally over long distances by ocean currents before it reaches the surface mixed layer, where it can contribute to the sea-air flux. In this context, MOx can serve as a key control mechanism, regulating methane's fate in the water column (Nordam et al., 2025; Dølven et al., 2025).

Given the strong regional methane variability observed in this study (Fig. 4, Fig. S2), extrapolating point-based rate measurements to basin-scale methane budgets introduces substantial uncertainty (Gründger et al., 2021; Silyakova et al., 2020; Steinle et al., 2015). Accurately assessing Arctic methane emissions, therefore, requires more in-depth studies that couple high-resolution MOx measurements, advanced genetic analyses, and hydrographic models that account for regional differences in microbial oxidation efficiency.

Methane dynamics in the Arctic marine environment are governed by an interplay between methane seep intensity, hydrographic structure, and MOx capacity. While active seep systems in the Barents Sea generate high bottom-water methane concentrations and strong vertical gradients, the fate of this methane is modulated by MOx efficiency. In hotspot areas with rich benthic diversity, such as the Crater area and the Pingo site in Storfjordrenna (e.g., Åström et al., 2020; Sen et al., 2018), enhanced microbial oxidation appears to act as an effective biological filter, substantially reducing methane before it can be ventilated to the sea surface. Although water-column MOx is not directly associated with benthic diversity, seep-associated fauna such as tube worms may indirectly promote methane oxidation by modifying sediment geochemistry, for example, through irrigation that transports oxygen and sulphate into deeper sediment layers, thereby creating favourable niches for aerobic methanotrophs and anaerobic methanotrophic archaea (Åström et al., 2018; Hong et al., 2017; Sen et al., 2018). In contrast, regions characterised by stronger circulation, advection, and vertical mixing, such as PKF and Lofoten, may inhibit the establishment of stable methanotrophic communities,

https://doi.org/10.5194/egusphere-2026-3607
Preprint. Discussion started: 30 June 2026


thereby reducing oxidation efficiency. Under these more dynamic hydrographic conditions, a larger fraction of dissolved methane may persist in the water column and potentially reach the surface layer before being oxidised.

### 5.3 Effect of methane on water biogeochemistry

Measurements showed substantial variability for most of the parameters within the shallow water column, particularly at coastal stations and in the near-surface layers, where hydrological processes are highly dynamic (Table 2, Fig. S1). Vertical profiles became markedly more uniform below the euphotic zone (Fig. 3). In these deeper layers, water masses were more stable and less influenced by short-term atmospheric forcing or freshwater inputs. This vertical homogeneity was especially pronounced at offshore stations where water depths exceeded 500 m, as well as at MAR stations, where depths reached approximately 4000 m (Fig. 3).

Nutrient distributions showed clear depth-dependent and spatial patterns closely linked to primary production. Concentrations were strongly depleted in surface waters due to biological uptake and gradually increased with depth as a result of remineralisation in deeper layers (Fig. 3). In contrast, particulate and dissolved organic matter accumulated primarily within the photic zone, reflecting photosynthesis-driven production and enhanced biological activity in surface waters. This pattern was also evident in the stoichiometric relationships among these parameters, which exhibited strong linear correspondences across comparisons, indicating tightly coupled production and recycling processes throughout the study regions (Fig. 6).

Our results are consistent with previous observations demonstrating strong nitrate depletion and nutrient limitation of primary production in Arctic waters, despite pronounced light limitation during winter (Codispoti et al., 2013; Randelhoff et al., 2020). However, most of our cruises were conducted during the summer months, primarily in June and July, after the major spring bloom had already occurred. As a result, surface nutrients had largely been consumed by phytoplankton production, while particulate organic matter had accumulated in the upper water column. By this time, freshwater input and vertical mixing had also weakened relative to earlier, allowing the development of a more stratified water column at most stations. Consequently, our data set captures relatively stable summer conditions and lacks a strong seasonal signal across both continental margin and offshore regions (Table 2, Fig. 3). This post-bloom signature was particularly evident in pronounced silicate depletion, reflecting earlier diatom-dominated production prior to the establishment of the summer stratified water column (Erga et al., 2014). Correspondingly, nitrogen depletion was also apparent in particulate matter stoichiometry, where measured elemental ratios deviated from the classical Redfield ratio (Redfield, 1958) and were instead closer to the revised ratios proposed later (Frigstad et al., 2011; Sterner et al., 2008).

Methane released from Arctic seeps is biologically available to a relatively limited functional group of microorganisms, primarily MOB. In the absence of an active methanotrophic community, methane behaves largely as a chemically inert compound in oxic seawater. Consequently, any alteration in water-column biogeochemistry associated with methane enrichment is ultimately mediated by methane oxidation to carbon dioxide or by the metabolic activity and biomass production of MOB. In the present study, together with previous investigations, we evaluated whether methane enrichment produces detectable changes in water-column biogeochemistry and which biogeochemical components might respond to elevated methane concentrations.

Both the data presented here and prior studies on organic matter biogeochemistry in the presented area indicate that methane does not directly alter nutrient regimes in the water column (Pohlman et al., 2009; Sert et al., 2020, 2022). Instead, its influence appears

https://doi.org/10.5194/egusphere-2026-3607
Preprint. Discussion started: 30 June 2026


to be structural rather than stoichiometric, potentially affecting microbial community composition and organic matter cycling rather than bulk nutrient concentrations. A primary reason for this limited impact is the relative concentration scale: even at the highest observed methane levels (on the order of several micromolar), nutrient and DOC concentrations are typically one to two orders of magnitude higher (Table 2). As a result, methane-derived carbon represents only a minor fraction of the total biogeochemical pools, rendering its effect on nutrient dynamics negligible in snapshot observations.

However, while instantaneous concentration effects appear minimal, methane flux at active seep sites is continuous, even though individual seeps have been shown to be intermittent (Ferré et al., 2024; Römer et al., 2016). Under hydrographic conditions that allow accumulation or lateral transport, sustained methane input could exert measurable biogeochemical effects over longer temporal scales (Boetius and Wenzhöfer, 2013; Pohlman et al., 2009). Therefore, although our results suggest that methane does not substantially perturb bulk nutrient dynamics in the short term, its cumulative impact on microbial processes and organic matter cycling may become significant under persistent seep activity and favourable retention conditions (Sert et al., 2025).

Overall, our results indicate that methane does not substantially alter the bulk nutrient regimes in the Arctic water column at present-day concentrations and hydrographic conditions. Even at micromolar levels near active seeps, methane represents a comparatively small carbon pool relative to dissolved organic and inorganic carbon and nutrients, limiting its direct impact on large-scale nutrient stoichiometry (Table 2). Instead, methane exerts a more subtle but potentially important structural influence on microbial communities and organic matter cycling. Elevated methane concentrations lead to more diverse and heterogeneous organic carbon compositions (Sert et al., 2020, 2023). Importantly, this effect cannot be attributed solely to MOB; rather, methane enrichment restructures microbial interactions, influences grazing dynamics, and increases the contribution of decaying biomass, thereby altering carbon biogeochemistry (Sert et al., 2023). Thus, while methane enrichment does not translate into measurable shifts in nutrient concentrations, it may modify the pathways and composition of carbon processing within the microbial food web.

## 6 Conclusion and perspectives

Water-column studies conducted during CAGE cruises between 2013 and 2023 have substantially advanced our understanding of methane dynamics in Arctic marine systems by demonstrating that methane fate is not controlled solely by seep intensity, but rather by the interplay among hydrography, microbial activity, and regional environmental conditions. Methane enrichment is generally confined to bottom waters near active seep sites, whereas concentrations in the upper water column are often low and close to background levels, reflecting rapid dilution, horizontal advection, and/or efficient removal processes. A key outcome of these studies is the recognition of strong regional variability in MOx, indicating that the efficiency of the pelagic microbial filter is highly site-specific and cannot be broadly generalised. At present-day concentrations, methane also appears to exert limited influence on bulk nutrient stoichiometry, suggesting that its primary role may instead occur through microbial pathways and carbon processing. Despite these advances, important knowledge gaps remain, particularly regarding the temporal variability of methane release, the controls and dynamics of MOx, and the transfer of methane-derived carbon into pelagic food webs and organic matter pools.

https://doi.org/10.5194/egusphere-2026-3607
Preprint. Discussion started: 30 June 2026


Building on the CAGE legacy, future research should adopt a more integrated framework linking seabed methane fluxes, water-column transport, microbial processes, and ecosystem-scale impacts within a rapidly changing Arctic system.

Future studies should also extend beyond observational water-column surveys of methane distributions and MOx rates. Controlled incubation experiments are essential for disentangling causal relationships and tracing the fate of methane-derived carbon under defined environmental conditions. Combining methane-enrichment incubations with high-resolution microbial community analyses and compound-specific carbon characterisation could directly track the incorporation of methane-derived carbon into biomass and dissolved organic matter pools. Integrating such experimental approaches within situ flux measurements and physical transport modelling would provide a more comprehensive understanding of how increasing methane release may influence biogeochemical cycling and carbon processing in the Arctic Ocean under future climate scenarios.

## Data and code availability

The data used in this paper are attached as Supplementary Material.

## Author contributions

MFS designed the study, performed data acquisition and wrote the manuscript with contributions from all coauthors.

## Competing Interests

The authors have the following competing interests: One of the coauthors is a member of the editorial board of Biogeosciences.

## Acknowledgements

This study is funded by the Research Council of Norway through CAGE (Centre for Gas Hydrate, Environment and Climate) project number 223259 and EMAN7 Environmental impact of Methane seepage and sub-seabed characterisation at LoVe-Node 7 project number 320100. We want to acknowledge the scientific and operational crew of R/V Helmer Hanssen and R/V Kronprins Haakon during CAGE cruises. We would like to acknowledge Jürgen Mienert for his contribution to the earlier version of the manuscript.

## References

Aagaard, K., Foldvik, A., and Hillman, S. R.: The West Spitsbergen Current: Disposition and water mass transformation, Journal of Geophysical Research: Oceans, 92, 3778–3784, https://doi.org/10.1029/JC092iC04p03778, 1987.

https://doi.org/10.5194/egusphere-2026-3607
Preprint. Discussion started: 30 June 2026


Andreassen, K.: CAGE14-3 Cruise Report: Marine Geological Cruise to Storfjordrenna and Bjørnøyrenna, CAGE – Centre for Arctic Gas Hydrate, Environment and Climate Report Series, 2, https://doi.org/10.7557/cage.6920, 2014.

Andreassen, K.: CAGE15-5 Cruise Report: Marine Geological Cruise to Storfjordrenna, Bjørnøyrenna and Thor Iversenbanken, CAGE – Centre for Arctic Gas Hydrate, Environment and Climate Report Series, 3, https://doi.org/10.7557/cage.6937, 2015.

Andreassen, K.: CAGE16-2 Cruise Report: Marine Geological Cruise to the Maud Basin and Crater Area, Bjørnøyrenna, CAGE – Centre for Arctic Gas Hydrate, Environment and Climate Report Series, 4, https://doi.org/10.7557/cage.6925, 2016.

Andreassen, K., Hubbard, A., Winsborrow, M., Patton, H., Vadakkepuliyambatta, S., Plaza-Faverola, A., Gudlaugsson, E., Serov, P., Deryabin, A., Mattingsdal, R., Mienert, J., and Bünz, S.: Massive blow-out craters formed by hydrate-controlled methane expulsion from the Arctic seafloor, Science, 356, 948–953, https://doi.org/10.1126/science.aal4500, 2017.

Andreassen, K., Patton, H., Mattingsdal, R., Moser, M., Cooke, F. A., Jansson, P., and Argentino, C.: CAGE19-2 Cruise Report: Hunting gas flares and launching seafloor observatory, CAGE – Centre for Arctic Gas Hydrate, Environment and Climate Report Series, 7, https://doi.org/10.7557/cage.6910, 2019.

CAGE – Centre for Arctic Gas Hydrate, Environment and Climate Report Series: https://septentrio.uit.no/index.php/cage/issue/archive, last access: 30 March 2026.

CAGE's interactive geodata web map: https://geodata.uit.no/cage_web_map, last access: 30 March 2026.

Argentino, C., Fallati, L., Petters, S., Bernstein, H. C., Barrenechea Angeles, I., Corrales-Guerrero, J., Savini, A., Ferré, B., and Panieri, G.: Seafloor chemosynthetic habitats and AOM-influenced sediment microbiome at a cold-water coral site off the Vesterålen coast, northern Norway, EGUsphere, 2025, 1–25, https://doi.org/10.5194/egusphere-2025-3906, 2025.

Åström, E., Carroll, M., Ambrose, W., and Carroll, J.: Arctic cold seeps in marine methane hydrate environments: impacts on shelf macrobenthic community structure offshore Svalbard, Marine Ecology Progress Series, 552, 1–18, https://doi.org/10.3354/meps11773, 2016.

Åström, E. K. L., Carroll, M. L., Ambrose, W. G., Sen, A., Silyakova, A., and Carroll, J.: Methane cold seeps as biological oases in the high-Arctic deep sea, Limnology and Oceanography, 63, S209–S231, https://doi.org/10.1002/lno.10732, 2018.

Åström, E. K. L., Sen, A., Carroll, M. L., and Carroll, J.: Cold Seeps in a Warming Arctic: Insights for Benthic Ecology, Frontiers in Marine Science, 7, 244, https://doi.org/10.3389/fmars.2020.00244, 2020.

Berchet, A., Bousquet, P., Pison, I., Locatelli, R., Chevallier, F., Paris, J.-D., Dlugokencky, E. J., Laurila, T., Hatakka, J., Viisanen, Y., Worthy, D. E. J., Nisbet, E., Fisher, R., France, J., Lowry, D., Ivakhov, V., and Hermansen, O.: Atmospheric constraints on the methane emissions from the East Siberian Shelf, Atmospheric Chemistry and Physics, 16, 4147–4157, https://doi.org/10.5194/acp-16-4147-2016, 2016.

Berndt, C., Feseker, T., Treude, T., Krastel, S., Liebetrau, V., Niemann, H., Bertics, V. J., Dumke, I., Dünnbier, K., Ferré, B., Graves, C., Gross, F., Hissmann, K., Hühnerbach, V., Krause, S., Lieser, K., Schauer, J., and Steinle, L.: Temporal Constraints on Hydrate-Controlled Methane Seepage off Svalbard, Science, 343, 284–287, https://doi.org/10.1126/science.1246298, 2014.

Biastoch, A., Treude, T., Rüpke, L. H., Riebesell, U., Roth, C., Burwicz, E. B., Park, W., Latif, M., Böning, C. W., Madec, G., and Wallmann, K.: Rising Arctic Ocean temperatures cause gas hydrate destabilization and ocean acidification, Geophysical Research Letters, 38, n/a-n/a, https://doi.org/10.1029/2011GL047222, 2011.

https://doi.org/10.5194/egusphere-2026-3607
Preprint. Discussion started: 30 June 2026


Boetius, A. and Wenzhöfer, F.: Seafloor oxygen consumption fuelled by methane from cold seeps, Nature Geoscience, 6, 725–734, https://doi.org/10.1038/ngeo1926, 2013.

Böttner, C., Jakobsen, F. W., Nielsen, T., Winsborrow, M., Polteau, S., Mazzini, A., Planke, S., Andresen, K. J., Millinge, O. J. S., Asif, M. R., Laberg, J. S., Hopper, J., Myklebust, R., and Seidenkrantz, M.-S.: Natural hydrocarbon seepage at the Northeast Greenland continental shelf, Commun Earth Environ, 6, 879, https://doi.org/10.1038/s43247-025-02932-8, 2025.

Bünz, S.: CAGE17-3 Cruise report, CAGE – Centre for Arctic Gas Hydrate, Environment and Climate Report Series, 5, https://doi.org/10.7557/cage.6952, 2017.

Bünz, S.: CAGE18-4 Cruise Report, CAGE – Centre for Arctic Gas Hydrate, Environment and Climate Report Series, 6, https://doi.org/10.7557/cage.6850, 2018.

Bünz, S. and Panieri, G.: CAGE14-1 Cruise Report: CAGE research school in Arctic Marine Geology and Geophysics, CAGE – Centre for Arctic Gas Hydrate, Environment and Climate Report Series, 2, https://doi.org/10.7557/cage.6898, 2014.

Bünz, S. and Ramirez-Llodra, E.: Hot Vents in an Ice-Covered Ocean - HACON21 expedition, CAGE – Centre for Arctic Gas Hydrate, Environment and Climate Report Series, 9, https://doi.org/10.7557/cage.6715, 2021.

Bünz, S., Polyanov, S., Vadakkepuliyambatta, S., Consolaro, C., and Mienert, J.: Active gas venting through hydrate-bearing sediments on the Vestnesa Ridge, offshore W-Svalbard, Marine Geology, 332–334, 189–197, https://doi.org/10.1016/j.margeo.2012.09.012, 2012.

Bünz, S., Vadakkepuliyambatta, S., Serov, P., Lepland, A., Himmler, T., Hong, W.-L., Lindgren, M., Moser, M., Jansson, P., Ferre, B., Svenning, M., Dimitri, K., Carrier, V., Geslin, E., Schmidt, C., Lucchi, R., and Mattingsdal, R.: CAGE18-5 Cruise report : Remotely-operated vehicle (ROV) investigations of active gas seepage sites in the Barents Sea, CAGE – Centre for Arctic Gas Hydrate, Environment and Climate Report Series, 6, https://doi.org/10.7557/cage.6853, 2018.

Bünz, S., Ramirez-Llodra, E., German, C., Ferre, B., Sert, F., Kalenickenko, D., Reeves, E., Hand, K., Dahle, H., Kutti, T., Purser, A., Hilario, A., Ramalho, S., Rapp, H. T., Ribeiro, P., Victorero, L., Hoge, U., Panieri, G., Bowen, A., Jakuba, M., Suman, S., Gomez-Ibanez, D., Judge, C., Curran, M., Nalicki, V., Vagenes, S., Lamar, L., Klesh, A., Dessandier, P. A., Steen, I., Mall, A., Vulcano, F., Meckel, E. M., and Drake, N.: RV Kronprins Håkon (cruise no. 2019708) Longyearbyen – Longyearbyen 19.09. – 16.10.2019, UIT - The Arctic University of Norway, 100 pp., 2020.

Carroll, M. L.: CAGE16-5 Cruise Report: ROV-based Geological and Biological Investigations of Methane Seeps at Prins Karls Forland, Storfjordrenna Pingos and Bjørnøyrenna Craters, CAGE – Centre for Arctic Gas Hydrate, Environment and Climate Report Series, 4, https://doi.org/10.7557/cage.6928, 2016.

Codispoti, L. A., Kelly, V., Thessen, A., Matrai, P., Suttles, S., Hill, V., Steele, M., and Light, B.: Synthesis of primary production in the Arctic Ocean: III. Nitrate and phosphate based estimates of net community production, Progress in Oceanography, 110, 126–150, https://doi.org/10.1016/j.pocean.2012.11.006, 2013.

Crespo-Medina, M., Meile, C. D., Hunter, K. S., Diercks, A.-R., Asper, V. L., Orphan, V. J., Tavormina, P. L., Nigro, L. M., Battles, J. J., Chanton, J. P., Shiller, A. M., Joung, D.-J., Amon, R. M. W., Bracco, A., Montoya, J. P., Villareal, T. A., Wood, A. M., and Joye, S. B.: The rise and fall of methanotrophy following a deepwater oil-well blowout, Nature Geoscience, 7, 423, https://doi.org/10.1038/ngeo2156, 2014.

Damm, E., Kiene, R. P., Schwarz, J., Falck, E., and Dieckmann, G.: Methane cycling in Arctic shelf water and its relationship with phytoplankton biomass and DMSP, Marine Chemistry, 109, 45–59, https://doi.org/10.1016/j.marchem.2007.12.003, 2008.

https://doi.org/10.5194/egusphere-2026-3607
Preprint. Discussion started: 30 June 2026


DeMets, C., Gordon, R., and Argus, D.: Geological current plate motions, GEOPHYS J INT, 181, 1–80, https://doi.org/10.1111/j.1365-246X.2009.04491.x, 2010.

Dessandier, P.-A., Panieri, G., Borrelli, C., and Kalenitchenko, D.: Benthic foraminifera in Arctic methane hydrate bearing sediments, Front. Mar. Sci., 6, https://doi.org/10.3389/fmars.2019.00765, 2019.

Dissanayake, A. L., Gros, J., Drews, H. J., Nielsen, J. W., and Drews, A.: Fate of Methane from the Nord Stream Pipeline Leaks, Environ. Sci. Technol. Lett., 10, 903–908, https://doi.org/10.1021/acs.estlett.3c00493, 2023.

Dølven, K. O.: Replication data for Autonomous methane seep site monitoring offshore Western Svalbard: Hourly to seasonal variability and associated oceanographic parameters, https://doi.org/10.18710/CEIA1U, 2023.

Dølven, K. O., Espenes, H., Hanssen, A., Sert, M. F., Drivdal, M., Randelhoff, A., and Ferré, B.: Modeling water column gas transformation, migration and atmospheric flux from seafloor seepage, Ocean Science, 21, 3031–3054, https://doi.org/10.5194/os-21-3031-2025, 2025.

Egger, M., Riedinger, N., Mogollón, J. M., and Jørgensen, B. B.: Global diffusive fluxes of methane in marine sediments, Nature Geosci, 11, 421–425, https://doi.org/10.1038/s41561-018-0122-8, 2018.

Erga, S. R., Ssebiyonga, N., Hamre, B., Frette, Ø., Rey, F., and Drinkwater, K.: Nutrients and phytoplankton biomass distribution and activity at the Barents Sea Polar Front during summer near Hopen and Storbanken, Journal of Marine Systems, 130, 181–192, https://doi.org/10.1016/j.jmarsys.2012.12.008, 2014.

Fer, I., Skogseth, R., Haugan, P. M., and Jaccard, P.: Observations of the Storfjorden overflow, Deep Sea Research Part I: Oceanographic Research Papers, 50, 1283–1303, https://doi.org/10.1016/S0967-0637(03)00124-9, 2003.

Fer, I., Müller, M., and Peterson, A. K.: Tidal forcing, energetics, and mixing near the Yermak Plateau, Ocean Sci., 11, 287–304, https://doi.org/10.5194/os-11-287-2015, 2015.

Ferré, B.: CAGE17-4 Cruise Report: Recovery of observatory and water column survey offshore Svalbard, CAGE – Centre for Arctic Gas Hydrate, Environment and Climate Report Series, 5, https://doi.org/10.7557/cage.6953, 2017.

Ferré, B.: CAGE18-2 Cruise Report: LoVe site – exploration around node 7, CAGE – Centre for Arctic Gas Hydrate, Environment and Climate Report Series, 6, https://doi.org/10.7557/cage.6770, 2018.

Ferré, B., Niemann, H., Jansson, P., Serov, P., Arnardottir, E. O., Tigreros, F. G., Leonte, M., Graves, C., and Hermundsplass, P. I.: CAGE16-4 Cruise Report: Recovery of observatories and water column survey offshore Svalbard, CAGE – Centre for Arctic Gas Hydrate, Environment and Climate Report Series, 4, https://doi.org/10.7557/cage.6927, 2016a.

Ferré, B., Portmov, A., Jansson, P., Axaopoulos, P., Frank, C., Sorensen, R., and Olsen, B. R.: CAGE16-7 Cruise Report: Deployment of observatories and water column survey in the Barents Sea and offshore Svalbard, CAGE – Centre for Arctic Gas Hydrate, Environment and Climate Report Series, 4, https://doi.org/10.7557/cage.6930, 2016b.

Ferré, B., Kalenitchenko, D., Moser, M., Stetzler, M., Holm, T., and Jensen, S.: CAGE20-1 Cruise Report: K-lander recovery and water column survey offshore Svalbard and in the Barents Sea, CAGE – Centre for Arctic Gas Hydrate, Environment and Climate Report Series, 8, https://doi.org/10.7557/cage.6912, 2020a.

Ferré, B., Panieri, G., Kalenitchenko, D., Argentino, C., Moser, M., Dølven, K. O., Sert, M. F., Stetzler, M., Savini, A., Lindgren, M., Jones, E., Groot, T. de, Friedrich, J., Jensen, S. A., Vågenes, S., Meyer, J. P., Micheel, M., and Erntsen, E.: CAGE20-7 Cruise

Report: Sediment and water column analyses around flares at Norskebanken, Hinlopen and offshore Prins Karls Forland, CAGE – Centre for Arctic Gas Hydrate, Environment and Climate Report Series, 8, https://doi.org/10.7557/cage.6916, 2020b.

Ferré, B., Jansson, P. G., Moser, M., Serov, P., Portnov, A., Graves, C. A., Panieri, G., Gründger, F., Berndt, C., Lehmann, M. F., and Niemann, H.: Reduced methane seepage from Arctic sediments during cold bottom-water conditions, Nat. Geosci., 13, 144–148, https://doi.org/10.1038/s41561-019-0515-3, 2020c.

Ferré, B., Panieri, G., Argentino, C., Sert, M. F., Stetzler, M., Fallati, L., Dills, M. S., Petters, S., Rohan, T., Barreyre, T., Lien, M. E., Kutti, T., Corrales, J., Kjær, M., Ting, R., Bojesen, M. D., Walta, A., and Jensen, S.: CAGE22-3 Cruise Report: EMAN7 cruise, CAGE – Centre for Arctic Gas Hydrate, Environment and Climate Report Series, 10, https://doi.org/10.7557/cage.6760, 2022.

Ferré, B., Barreyre, T., Bünz, S., Argentino, C., Corrales-Guerrero, J., Dølven, K. O., Stetzler, M., Fallati, L., Sert, M. F., Panieri, G., Rastrick, S., Kutti, T., and Moser, M.: Contrasting Methane Seepage Dynamics in the Hola Trough Offshore Norway: Insights From Two Different Summers, Journal of Geophysical Research: Oceans, 129, e2024JC020949, https://doi.org/10.1029/2024JC020949, 2024.

Frigstad, H., Andersen, T., Hessen, D. O., Naustvoll, L.-J., Johnsen, T. M., and Bellerby, R. G. J.: Seasonal variation in marine C:N:P stoichiometry: can the composition of seston explain stable Redfield ratios?, Biogeosciences, 8, 2917–2933, https://doi.org/10.5194/bg-8-2917-2011, 2011.

Geissler, W. H., Gebhardt, A. C., Gross, F., Wollenburg, J., Jensen, L., Schmidt-Aursch, M. C., Krastel, S., Elger, J., and Osti, G.: Arctic megaslide at presumed rest, Sci Rep, 6, 38529, https://doi.org/10.1038/srep38529, 2016.

Grasshoff, K., Ehrhardt, M., Kremling, K., and Anderson, L. G. (Eds.): Methods of seawater analysis, 3rd, completely rev. and extended ed ed., Wiley-VCH, Weinheim ; New York, 600 pp., 1999.

Graves, C. A., Steinle, L., Rehder, G., Niemann, H., Connelly, D. P., Lowry, D., Fisher, R. E., Stott, A. W., Sahling, H., and James, R. H.: Fluxes and fate of dissolved methane released at the seafloor at the landward limit of the gas hydrate stability zone offshore western Svalbard: Dissolved methane off western Svalbard, Journal of Geophysical Research: Oceans, 120, 6185–6201, https://doi.org/10.1002/2015JC011084, 2015.

Greinert, J., Pohlman, J., Silyakova, A., Mienert, J., Ruppel, C., and Casso, M.: Atmospheric methane emissions coupled to a CO2-sink at an Arctic shelf seep area offshore NW Svalbard: Introducing the" Seep-Fertilization Hypothesis", in: EGU General Assembly Conference Abstracts, 10015, 2015.

de Groot, T. R., Kalenitchenko, D., Moser, M., Argentino, C., Panieri, G., Lindgren, M., Dølven, K. O., Ferré, B., Svenning, M. M., and Niemann, H.: Methanotroph activity and connectivity between two seep systems north off Svalbard, Front. Earth Sci., 12, https://doi.org/10.3389/feart.2024.1287226, 2024.

Gründger, F., Probandt, D., Knittel, K., Carrier, V., Kalenitchenko, D., Silyakova, A., Serov, P., Ferré, B., Svenning, M. M., and Niemann, H.: Seasonal shifts of microbial methane oxidation in Arctic shelf waters above gas seeps, Limnology and Oceanography, n/a, https://doi.org/10.1002/lno.11731, 2021.

Hanson, R. S. and Hanson, T. E.: Methanotrophic bacteria., Microbiological reviews, 60, 439–471, 1996.

Hong, W.-L., Torres, M. E., Carroll, J., Crémière, A., Panieri, G., Yao, H., and Serov, P.: Seepage from an arctic shallow marine gas hydrate reservoir is insensitive to momentary ocean warming, Nat Commun, 8, 15745, https://doi.org/10.1038/ncomms15745, 2017.

https://doi.org/10.5194/egusphere-2026-3607
Preprint. Discussion started: 30 June 2026


Jakobsson, M., Mayer, L., Coakley, B., Dowdeswell, J. A., Forbes, S., Fridman, B., Hodnesdal, H., Noormets, R., Pedersen, R., Rebesco, M., Schenke, H. W., Zarayskaya, Y., Accettella, D., Armstrong, A., Anderson, R. M., Bienhoff, P., Camerlenghi, A., Church, I., Edwards, M., Gardner, J. V., Hall, J. K., Hell, B., Hestvik, O., Kristoffersen, Y., Marcussen, C., Mohammad, R., Mosher, D., Nghiem, S. V., Pedrosa, M. T., Travaglini, P. G., and Weatherall, P.: The International Bathymetric Chart of the Arctic Ocean (IBCAO) Version 3.0: IBCAO VERSION 3.0, Geophysical Research Letters, 39, n/a-n/a, https://doi.org/10.1029/2012GL052219, 2012.

James, R. H., Bousquet, P., Bussmann, I., Haeckel, M., Kipfer, R., Leifer, I., Niemann, H., Ostrovsky, I., Piskozub, J., Rehder, G., Treude, T., Vielstädte, L., and Greinert, J.: Effects of climate change on methane emissions from seafloor sediments in the Arctic Ocean: A review, Limnology and Oceanography, 61, S283–S299, https://doi.org/10.1002/lno.10307, 2016.

Jansson, P., Ferré, B., Silyakova, A., Dølven, K. O., and Omstedt, A.: A new numerical model for understanding free and dissolved gas progression toward the atmosphere in aquatic methane seepage systems: Marine two-phase gas model in one dimension, Limnology and Oceanography: Methods, https://doi.org/10.1002/lom3.10307, 2019.

Johnson, J. E., Mienert, J., Plaza-Faverola, A., Vadakkepuliyambatta, S., Knies, J., Bünz, S., Andreassen, K., and Ferré, B.: Abiotic methane from ultraslow-spreading ridges can charge Arctic gas hydrates, Geology, 43, 371–374, https://doi.org/10.1130/G36440.1, 2015.

Judd, A. and Hovland, M. (Eds.): The nature and origins of flowing fluids, in: Seabed Fluid Flow: The Impact on Geology, Biology and the Marine Environment, Cambridge University Press, Cambridge, 144–162, https://doi.org/10.1017/CBO9780511535918.007, 2007.

Keir, R. S., Greinert, J., Rhein, M., Petrick, G., Sültenfuß, J., and Fürhaupter, K.: Methane and methane carbon isotope ratios in the Northeast Atlantic including the Mid-Atlantic Ridge (50°N), Deep Sea Research Part I: Oceanographic Research Papers, 52, 1043–1070, https://doi.org/10.1016/j.dsr.2004.12.006, 2005.

Kolomijeca, A., Marx, L., Reynolds, S., Cariou, T., Mawji, E., and Boulart, C.: An update on dissolved methane distribution in the subtropical North Atlantic Ocean, Ocean Science, 18, 1377–1388, https://doi.org/10.5194/os-18-1377-2022, 2022.

Loeng, H.: Features of the physical oceanographic conditions of the Barents Sea, Polar Research, 10, 5–18, https://doi.org/10.3402/polar.v10i1.6723, 1991.

Magen, C., Lapham, L. L., Pohlman, J. W., Marshall, K., Bosman, S., Casso, M., and Chanton, J. P.: A simple headspace equilibration method for measuring dissolved methane, Limnology and Oceanography: Methods, 12, 637–650, https://doi.org/10.4319/lom.2014.12.637, 2014.

Marcon, Y., Stetzler, M., Ferré, B., Kopiske, E., and Bohrmann, G.: Deep learning-based characterization of underwater methane bubbles using simple dual camera platform, Limnology and Oceanography: Methods, 23, 155–175, https://doi.org/10.1002/lom3.10672, 2025.

Mau, S., Blees, J., Helmke, E., Niemann, H., and Damm, E.: Vertical distribution of methane oxidation and methanotrophic response to elevated methane concentrations in stratified waters of the Arctic fjord Storfjorden (Svalbard, Norway), Biogeosciences, 10, 6267–6278, https://doi.org/10.5194/bg-10-6267-2013, 2013.

Mau, S., Römer, M., Torres, M. E., Bussmann, I., Pape, T., Damm, E., Geprägs, P., Wintersteller, P., Hsu, C.-W., Loher, M., and Bohrmann, G.: Widespread methane seepage along the continental margin off Svalbard - from Bjørnøya to Kongsfjorden, Scientific Reports, 7, 42997, https://doi.org/10.1038/srep42997, 2017.

https://doi.org/10.5194/egusphere-2026-3607
Preprint. Discussion started: 30 June 2026


McGinnis, D. F., Greinert, J., Artemov, Y., Beaubien, S. E., and Wüest, A.: Fate of rising methane bubbles in stratified waters: How much methane reaches the atmosphere?, Journal of Geophysical Research: Oceans, 111, https://doi.org/10.1029/2005JC003183, 2006.

Menze, S., Ingvaldsen, R. B., Nikolopoulos, A., Hattermann, T., Albretsen, J., and Gjøsæter, H.: Productive detours – Atlantic water inflow and acoustic backscatter in the major troughs along the Svalbard shelf, Progress in Oceanography, 188, 102447, https://doi.org/10.1016/j.pocean.2020.102447, 2020.

Mienert, J., Hong, W.-L., Jansson, P., Waghorn, K. A., Waage, M., Singhroha, S., Osti, G., Yao, H., Iversen, S., Olsen, B. R., Heimdal, K., Krokmyrdal, S., Romeyn, R., Triest, J., and Grilli, R.: CAGE15-6 Cruise Report: Arctic gas hydrate studies, CAGE – Centre for Arctic Gas Hydrate, Environment and Climate Report Series, 3, https://doi.org/10.7557/cage.6939, 2015.

Mienert, J., Berndt, C., Tréhu, A. M., Camerlenghi, A., and Liu, C.-S. (Eds.): World Atlas of Submarine Gas Hydrates in Continental Margins, Springer International Publishing, Cham, https://doi.org/10.1007/978-3-030-81186-0, 2022.

Myhre, C. L., Ferré, B., Platt, S. M., Silyakova, A., Hermansen, O., Allen, G., Pisso, I., Schmidbauer, N., Stohl, A., Pitt, J., Jansson, P., Greinert, J., Percival, C., Fjaeraa, A. M., O'Shea, S. J., Gallagher, M., Le Breton, M., Bower, K. N., Bauguitte, S. J. B., Dalsøren, S., Vadakkepuliyambatta, S., Fisher, R. E., Nisbet, E. G., Lowry, D., Myhre, G., Pyle, J. A., Cain, M., and Mienert, J.: Extensive release of methane from Arctic seabed west of Svalbard during summer 2014 does not influence the atmosphere, Geophys. Res. Lett., 43, 2016GL068999, https://doi.org/10.1002/2016GL068999, 2016.

Niemann, H., Steinle, L., Blees, J., Bussmann, I., Treude, T., Krause, S., Elvert, M., and Lehmann, M. F.: Toxic effects of lab-grade butyl rubber stoppers on aerobic methane oxidation, Limnology and Oceanography: Methods, 13, 40–52, https://doi.org/10.1002/lom3.10005, 2015.

Nilsen, F., Skogseth, R., Vaardal-Lunde, J., and Inall, M.: A Simple Shelf Circulation Model: Intrusion of Atlantic Water on the West Spitsbergen Shelf, Journal of Physical Oceanography, 46, 1209–1230, https://doi.org/10.1175/JPO-D-15-0058.1, 2016.

Nisbet, E. G.: Methane's unknowns better known, Nat. Geosci., 15, 861–862, https://doi.org/10.1038/s41561-022-01049-3, 2022.

Nordam, T., Dissanayake, A. L., Brakstad, O. G., Hakvåg, S., Øverjordet, I. B., Litzler, E., Nepstad, R., Drews, A., and Röhrs, J.: Fate of Dissolved Methane from Ocean Floor Seeps, Environ. Sci. Technol., 59, 8516–8526, https://doi.org/10.1021/acs.est.5c03297, 2025.

Oziel, L., Sirven, J., and Gascard, J.-C.: The Barents Sea frontal zones and water masses variability (1980–2011), Ocean Science, 12, 169–184, https://doi.org/10.5194/os-12-169-2016, 2016.

Panieri, G., Bünz, S., Fornari, D. J., Escartin, J., Serov, P., Jansson, P., Torres, M. E., Johnson, J. E., Hong, W., Sauer, S., Garcia, R., and Gracias, N.: An integrated view of the methane system in the pockmarks at Vestnesa Ridge, 79°N, Marine Geology, 390, 282–300, https://doi.org/10.1016/j.margeo.2017.06.006, 2017a.

Panieri, G., Alexandropoulou, N., Bruvik, K. L., Carrier, V., Dessandier, P.-A., Dølven, K. O., Valberg, E., Fornari, D., Gründger, F., Kurras, G. J., Yao, H., Holm, T., Lindgren, M., Melaniuk, K., Olsen, B. R., Ofstad, S., Patton, H., Romeyn, R., Sauer, S., Sen, A., and Sert, M.: CAGE17-2 Cruise Report: Gas hydrate deposits and methane seepages in Storfjordrenna, Northern Flank of Olga Basin, and West Sentralbanken (Barents Sea): Biogeochemical and biological investigations, CAGE – Centre for Arctic Gas Hydrate, Environment and Climate Report Series, 5, https://doi.org/10.7557/cage.6955, 2017b.

https://doi.org/10.5194/egusphere-2026-3607
Preprint. Discussion started: 30 June 2026


Patton, H., Mattingsdal, R., Pavel, S., Cooke, F. A., and Alexandropoulou, N.: CAGE20-2 Cruise Report: Hunting flares in Hopendjupet and glacigenic sediments in Sentralbankrenna, CAGE – Centre for Arctic Gas Hydrate, Environment and Climate Report Series, 8, https://doi.org/10.7557/cage.6745, 2020.

Platt, S. M.: Methane Emissions from the Arctic Ocean to the Atmosphere, in: Geophysical Research Abstracts, EGU, 2015.

Platt, S. M., Eckhardt, S., Ferré, B., Fisher, R. E., Hermansen, O., Jansson, P., Lowry, D., Nisbet, E. G., Pisso, I., Schmidbauer, N., Silyakova, A., Stohl, A., Svendby, T. M., Vadakkepuliyambatta, S., Mienert, J., and Lund Myhre, C.: Methane at Svalbard and over the European Arctic Ocean, Atmospheric Chemistry and Physics Discussions, 1–30, https://doi.org/10.5194/acp-2018-597, 2018.

Plaza-Faverola, A.: CAGE18-1 Cruise Report: Marine Geophysical Cruise to Storbanken and Olga Basin in the Barents Sea, CAGE – Centre for Arctic Gas Hydrate, Environment and Climate Report Series, 6, https://doi.org/10.7557/cage.6846, 2018.

Pohlman, J. W., Bauer, J. E., Canuel, E. A., Grabowski, K. S., Knies, D. L., Mitchell, C. S., Whiticar, M. J., and Coffin, R. B.: Methane sources in gas hydrate-bearing cold seeps: Evidence from radiocarbon and stable isotopes, Marine Chemistry, 115, 102–109, https://doi.org/10.1016/j.marchem.2009.07.001, 2009.

Portnov, A., Smith, A. J., Mienert, J., Cherkashov, G., Rekant, P., Semenov, P., Serov, P., and Vanshtein, B.: Offshore permafrost decay and massive seabed methane escape in water depths >20 m at the South Kara Sea shelf, Geophysical Research Letters, 40, 3962–3967, https://doi.org/10.1002/grl.50735, 2013.

Portnov, A., Mienert, J., and Serov, P.: Modeling the evolution of climate-sensitive Arctic subsea permafrost in regions of extensive gas expulsion at the West Yamal shelf, Journal of Geophysical Research: Biogeosciences, 119, 2082–2094, https://doi.org/10.1002/2014JG002685, 2014.

Portnov, A., Vadakkepuliyambatta, S., Mienert, J., and Hubbard, A.: Ice-sheet-driven methane storage and release in the Arctic, Nature Communications, 7, 10314, https://doi.org/10.1038/ncomms10314, 2016.

Qian, J. and Mopper, K.: Automated High-Performance, High-Temperature Combustion Total Organic Carbon Analyzer, Anal. Chem., 68, 3090–3097, https://doi.org/10.1021/ac960370z, 1996.

Randelhoff, A., Holding, J., Janout, M., Sejr, M. K., Babin, M., Tremblay, J.-É., and Alkire, M. B.: Pan-Arctic Ocean Primary Production Constrained by Turbulent Nitrate Fluxes, Front. Mar. Sci., 7, https://doi.org/10.3389/fmars.2020.00150, 2020.

Rasmussen, T. L., Nielsen, T., Zamelczyk, K., and Sztybor, K.: CAGE14-4 Cruise Report: CAGE-CO2 Cruise and GEO3144 Teaching Cruise to the western Svalbard margin and the Barents Sea, CAGE – Centre for Arctic Gas Hydrate, Environment and Climate Report Series, 2, https://doi.org/10.7557/cage.6921, 2014.

Rasmussen, T. L., Niemann, H., Gründger, F., Jansson, P., Sert, M. F., Serov, P., and Carrier, V.: CAGE17-1-Leg1 Cruise Report: Water column observation from CTD and water samples west of Prins Karls Forland, Svalbard, CAGE – Centre for Arctic Gas Hydrate, Environment and Climate Report Series, 5, https://doi.org/10.7557/cage.6941, 2017a.

Rasmussen, T. L., Nielsen, T., Laier, T., Olsen, B. R., Iversen, S., Sert, M., Jansson, P., and Serov, P.: CAGE17-1-Leg2 Cruise report, CAGE – Centre for Arctic Gas Hydrate, Environment and Climate Report Series, 5, https://doi.org/10.7557/cage.6954, 2017b.

Rastrick, S. S. P., Graham, H., Azetsu-Scott, K., Calosi, P., Chierici, M., Fransson, A., Hop, H., Hall-Spencer, J., Milazzo, M., Thor, P., and Kutti, T.: Using natural analogues to investigate the effects of climate change and ocean acidification on Northern ecosystems, ICES Journal of Marine Science, 75, 2299–2311, https://doi.org/10.1093/icesjms/fsy128, 2018.

https://doi.org/10.5194/egusphere-2026-3607
Preprint. Discussion started: 30 June 2026


Redfield, A. C.: The biological control of chemical factors in the environment, American Scientist, 46, 230A–221, 1958.

Reeburgh, W. S.: Oceanic Methane Biogeochemistry, Chem. Rev., 107, 486–513, https://doi.org/10.1021/cr050362v, 2007.

Römer, M., Riedel, M., Scherwath, M., Heesemann, M., and Spence, G. D.: Tidally controlled gas bubble emissions: A comprehensive study using long-term monitoring data from the NEPTUNE cabled observatory offshore Vancouver Island, Geochemistry, Geophysics, Geosystems, 17, 3797–3814, https://doi.org/10.1002/2016GC006528, 2016.

Rudels, B., Björk, G., Nilsson, J., Winsor, P., Lake, I., and Nohr, C.: The interaction between waters from the Arctic Ocean and the Nordic Seas north of Fram Strait and along the East Greenland Current: results from the Arctic Ocean-02 Oden expedition, Journal of Marine Systems, 55, 1–30, https://doi.org/10.1016/j.jmarsys.2004.06.008, 2005.

Ruppel, C. D. and Kessler, J. D.: The interaction of climate change and methane hydrates: Climate-Hydrates Interactions, Reviews of Geophysics, https://doi.org/10.1002/2016RG000534, 2017.

Sahling, H., Römer, M., Pape, T., Bergès, B., dos Santos Fereirra, C., Boelmann, J., Geprägs, P., Tomczyk, M., Nowald, N., Dimmler, W., Schroedter, L., Glockzin, M., and Bohrmann, G.: Gas emissions at the continental margin west of Svalbard: mapping, sampling, and quantification, Biogeosciences, 11, 6029–6046, https://doi.org/10.5194/bg-11-6029-2014, 2014.

Sauer, S., Hong, W.-L., Yao, H., Lepland, A., Klug, M., Eichinger, F., Himmler, T., Crémière, A., Panieri, G., Schubert, C. J., and Knies, J.: Methane transport and sources in an Arctic deep-water cold seep offshore NW Svalbard (Vestnesa Ridge, 79°N), Deep Sea Research Part I: Oceanographic Research Papers, 103430, https://doi.org/10.1016/j.dsr.2020.103430, 2020.

Schauer, U., Fahrbach, E., Osterhus, S., and Rohardt, G.: Arctic warming through the Fram Strait: Oceanic heat transport from 3 years of measurements, Journal of Geophysical Research: Oceans, 109, https://doi.org/10.1029/2003JC001823, 2004.

Schneider, A., Panieri, G., Lepland, A., Consolaro, C., Crémière, A., Forwick, M., Johnson, J. E., Plaza-Faverola, A., Sauer, S., and Knies, J.: Methane seepage at Vestnesa Ridge (NW Svalbard) since the Last Glacial Maximum, Quaternary Science Reviews, 193, 98–117, https://doi.org/10.1016/j.quascirev.2018.06.006, 2018.

Scranton, M. I. and Brewer, P. G.: Consumption of dissolved methane in the deep ocean, Limnology and Oceanography, 23, 1207–1213, 1978.

Sen, A., Åström, E. K. L., Hong, W.-L., Portnov, A., Waage, M., Serov, P., Carroll, M. L., and Carroll, J.: Geophysical and geochemical controls on the megafaunal community of a high Arctic cold seep, Biogeosciences, 15, 4533–4559, https://doi.org/10.5194/bg-15-4533-2018, 2018a.

Sen, A., Åström, E. K. L., Hong, W.-L., Portnov, A., Waage, M., Serov, P., Carroll, M. L., and Carroll, J.: Geophysical and geochemical controls on the megafaunal community of a high Arctic cold seep, Biogeosciences, 15, 4533–4559, https://doi.org/10.5194/bg-15-4533-2018, 2018b.

Serov, P., Portnov, A., Mienert, J., Semenov, P., and Ilatovskaya, P.: Methane release from pingo-like features across the South Kara Sea shelf, an area of thawing offshore permafrost, Journal of Geophysical Research: Earth Surface, 120, 1515–1529, https://doi.org/10.1002/2015JF003467, 2015.

Serov, P., Patton, H., Mazzini, A., Mattingsdal, R., Shephard, G., Cooke, F. A., Aguiar, V. C. M. de, Holm, V. D., Alessandrini, G., Cala, J. C. M., and Luerssen, P.: CAGE22-6 cruise report: GEO-3144/8144 Teaching Cruise: Geologically controlled hydrocarbon seepage in Hopendjupet and the wider Barents Sea, CAGE – Centre for Arctic Gas Hydrate, Environment and Climate Report Series, 10, https://doi.org/10.7557/cage.6769, 2022.

https://doi.org/10.5194/egusphere-2026-3607
Preprint. Discussion started: 30 June 2026


Serov, P., Andreassen, K., Winsborrow, M., Mattingsdal, R., and Patton, H.: Geological and glaciological controls of 21,700 active methane seeps in the northern Norwegian Barents sea, Front. Earth Sci., 12, https://doi.org/10.3389/feart.2024.1404027, 2024.

Sert, M. F., D'Andrilli, J., Gründger, F., Niemann, H., Granskog, M. A., Pavlov, A. K., Ferré, B., and Silyakova, A.: Compositional Differences in Dissolved Organic Matter Between Arctic Cold Seeps Versus Non-Seep Sites at the Svalbard Continental Margin and the Barents Sea, Front. Earth Sci., 8, 552731, https://doi.org/10.3389/feart.2020.552731, 2020.

Sert, M. F., Niemann, H., Reeves, E. P., Granskog, M. A., Hand, K. P., Kekäläinen, T., Jänis, J., Rossel, P. E., Ferré, B., Silyakova, A., and Gründger, F.: Compositions of dissolved organic matter in the ice-covered waters above the Aurora hydrothermal vent system, Gakkel Ridge, Arctic Ocean, Biogeosciences, 19, 2101–2120, https://doi.org/10.5194/bg-19-2101-2022, 2022.

Sert, M. F., Schweitzer, H. D., de Groot, T. R., Kekäläinen, T., Jänis, J., Bernstein, H. C., Ferré, B., Gründger, F., Kalenitchenko, D., and Niemann, H.: Elevated methane alters dissolved organic matter composition in the Arctic Ocean cold seeps, Frontiers in Earth Science, 11, 2023.

Sert, M. F., Bernstein, H. C., Dølven, K. O., Petters, S., Kekäläinen, T., Jänis, J., Corrales-Guerrero, J., and Ferré, B.: Cold Seeps and Coral Reefs in Northern Norway: Carbon Cycling in Marine Ecosystems With Coexisting Features, Journal of Geophysical Research: Biogeosciences, 130, e2024JG008475, https://doi.org/10.1029/2024JG008475, 2025.

Shakhova, N., Semiletov, I., Salyuk, A., Yusupov, V., Kosmach, D., and Gustafsson, Ö.: Extensive Methane Venting to the Atmosphere from Sediments of the East Siberian Arctic Shelf, Science, 327, 1246–1250, https://doi.org/10.1126/science.1182221, 2010.

Shakhova, N., Semiletov, I., Leifer, I., Sergienko, V., Salyuk, A., Kosmach, D., Chernykh, D., Stubbs, C., Nicolsky, D., Tumskoy, V., and Gustafsson, Ö.: Ebullition and storm-induced methane release from the East Siberian Arctic Shelf, Nature Geosci, 7, 64–70, https://doi.org/10.1038/ngeo2007, 2014.

Silyakova, A., Serov, P., Jansson, P., Gründger, F., Niemann, H., Graves, C., Arnadottir, E. O., Linke, P., Frank, C., Rubinke, O., Pohlman, J., Boze, L.-G., Magen, C., Tigrero, F. G., and Iversen, S.: CAGE15-3 Cruise Report, CAGE – Centre for Arctic Gas Hydrate, Environment and Climate Report Series, 3, https://doi.org/10.7557/cage.6933, 2015.

Silyakova, A., Jansson, P., Serov, P., Ferré, B., Pavlov, A. K., Hattermann, T., Graves, C. A., Platt, S. M., Myhre, C. L., Gründger, F., and Niemann, H.: Physical controls of dynamics of methane venting from a shallow seep area west of Svalbard, Continental Shelf Research, 194, 104030, https://doi.org/10.1016/j.csr.2019.104030, 2020.

Skogseth, R., Haugan, P. M., and Jakobsson, M.: Watermass transformations in Storfjorden, Continental Shelf Research, 25, 667–695, https://doi.org/10.1016/j.csr.2004.10.005, 2005.

Smith, A. J., Mienert, J., Bünz, S., and Greinert, J.: Thermogenic methane injection via bubble transport into the upper Arctic Ocean from the hydrate-charged Vestnesa Ridge, Svalbard, Geochemistry, Geophysics, Geosystems, 15, 1945–1959, https://doi.org/10.1002/2013GC005179, 2014.

Steinle, L., Graves, C. A., Treude, T., Ferré, B., Biastoch, A., Bussmann, I., Berndt, C., Krastel, S., James, R. H., Behrens, E., Böning, C. W., Greinert, J., Sapart, C.-J., Scheinert, M., Sommer, S., Lehmann, M. F., and Niemann, H.: Water column methanotrophy controlled by a rapid oceanographic switch, Nature Geoscience, 8, 378–382, https://doi.org/10.1038/ngeo2420, 2015.

Sterner, R. W., Andersen, T., Elser, J. J., Hessen, D. O., Hood, J. M., McCauley, E., and Urabe, J.: Scale-dependent carbon:nitrogen:phosphorus seston stoichiometry in marine and freshwaters, Limnology and Oceanography, 53, 1169–1180, https://doi.org/10.4319/lo.2008.53.3.1169, 2008.

https://doi.org/10.5194/egusphere-2026-3607
Preprint. Discussion started: 30 June 2026


Sultan, N., Plaza-Faverola, A., Vadakkepuliyambatta, S., Buenz, S., and Knies, J.: Impact of tides and sea-level on deep-sea Arctic methane emissions, Nat Commun, 11, 5087, https://doi.org/10.1038/s41467-020-18899-3, 2020.

Thorsnes, T., Chand, S., Bellec, V., Nixon, F. C., Brunstad, H., Lepland, A., and Aarrestad, S. M.: Gas seeps in Norwegian waters – distribution and mechanisms, Norwegian Journal of Geology, 103, https://doi.org/10.17850/njg103-2-4, 2023.

Thornton, B. F., Wik, M., and Crill, P. M.: Double-counting challenges the accuracy of high-latitude methane inventories, Geophysical Research Letters, 43, 12,569-12,577, https://doi.org/10.1002/2016GL071772, 2016.

Vanneste, M., Mienert, J., and Bünz, S.: The Hinlopen Slide: A giant, submarine slope failure on the northern Svalbard margin, Arctic Ocean, Earth and Planetary Science Letters, 245, 373–388, https://doi.org/10.1016/j.epsl.2006.02.045, 2006.

Veloso-Alarcón, M. E., Jansson, P., Batist, M. D., Minshull, T. A., Westbrook, G. K., Pälike, H., Bünz, S., Wright, I., and Greinert, J.: Variability of Acoustically Evidenced Methane Bubble Emissions Offshore Western Svalbard, Geophysical Research Letters, 46, 9072–9081, https://doi.org/10.1029/2019GL082750, 2019.

Waage, M., Portnov, A., Serov, P., Bünz, S., Waghorn, K. A., Vadakkepuliyambatta, S., Mienert, J., and Andreassen, K.: Geological Controls on Fluid Flow and Gas Hydrate Pingo Development on the Barents Sea Margin, Geochemistry, Geophysics, Geosystems, 20, 630–650, https://doi.org/10.1029/2018GC007930, 2019.

Wallmann, K., Riedel, M., Hong, W. L., Patton, H., Hubbard, A., Pape, T., Hsu, C. W., Schmidt, C., Johnson, J. E., Torres, M. E., Andreassen, K., Berndt, C., and Bohrmann, G.: Gas hydrate dissociation off Svalbard induced by isostatic rebound rather than global warming, Nat Commun, 9, 83, https://doi.org/10.1038/s41467-017-02550-9, 2018.

Westbrook, G. K., Thatcher, K. E., Rohling, E. J., Piotrowski, A. M., Pälike, H., Osborne, A. H., Nisbet, E. G., Minshull, T. A., Lanoisellé, M., James, R. H., Hühnerbach, V., Green, D., Fisher, R. E., Crocker, A. J., Chabert, A., Bolton, C., Beszczynska-Möller, A., Berndt, C., and Aquilina, A.: Escape of methane gas from the seabed along the West Spitsbergen continental margin, Geophysical Research Letters, 36, n/a-n/a, https://doi.org/10.1029/2009GL039191, 2009.

Winkelmann, D. and Stein, R.: Triggering of the Hinlopen/Yermak Megaslide in relation to paleoceanography and climate history of the continental margin north of Spitsbergen, Geochemistry, Geophysics, Geosystems, 8, https://doi.org/10.1029/2006GC001485, 2007.

Winkelmann, D., Jokat, W., Niessen, F., Stein, R., and Winkler, A.: Age and extent of the Yermak Slide north of Spitsbergen, Arctic Ocean, Geochemistry, Geophysics, Geosystems, 7, https://doi.org/10.1029/2005GC001130, 2006.

Winsborrow, M. and Knies, J.: CAGE21-6 Cruise Report: Hydrocarbon leakage in Hopendjupet, central Barents Sea, CAGE – Centre for Arctic Gas Hydrate, Environment and Climate Report Series, 9, https://doi.org/10.7557/cage.6675, 2021.

Winsborrow, M., Patton, H., Jakobsen, F., Pau, M., Akinselure, A., and Jensen, A.: CAGE21-4 Cruise Report: Oil slicks, gas flares and glacial landforms in Hopendjupet and Sentralbanken, CAGE – Centre for Arctic Gas Hydrate, Environment and Climate Report Series, 9, https://doi.org/10.7557/cage.6703, 2021.

Winsborrow et al. in prep.

Yao, H., Hong, W.-L., Panieri, G., Sauer, S., Torres, M. E., Lehmann, M. F., Gründger, F., and Niemann, H.: Fracture-controlled fluid transport supports microbial methaneoxidizing communities at the Vestnesa Ridge, Biogeosciences Discussions, 1–17, https://doi.org/10.5194/bg-2018-321, 2018.

https://doi.org/10.5194/egusphere-2026-3607
Preprint. Discussion started: 30 June 2026


915 Yao, H., Hong, W.-L., Panieri, G., Sauer, S., Torres, M. E., Lehmann, M. F., Gründger, F., and Niemann, H.: Fracture-controlled fluid transport supports microbial methane-oxidizing communities at Vestnesa Ridge, Biogeosciences, 16, 2221–2232, https://doi.org/10.5194/bg-16-2221-2019, 2019.

Yao, H., Panieri, G., Lehmann, M. F., Himmler, T., and Niemann, H.: Biomarker and Isotopic Composition of Seep Carbonates Record Environmental Conditions in Two Arctic Methane Seeps, Frontiers in Earth Science, 8, 755,
920 https://doi.org/10.3389/feart.2020.570742, 2021.